Inorganic Chemistry

Article

pubs.acs.org/IC

Accessing Ni(III)-Thiolate Versus Ni(II)-Thiyl Bonding in a Family of Ni−N_2S_2 Synthetic Models of NiSOD

Ellen P. Broering,[†] Stephanie Dillon,[‡] Eric M. Gale,[†] Ramsey A. Steiner,[†] Joshua Telser,[§] Thomas C. Brunold,[‡] and Todd C. Harrop*[,†]

[†]Department of Chemistry and Center for Metalloenzyme Studies, The University of Georgia, 1001 Cedar Street, Athens, Georgia 30602, United States

[‡]Department of Chemistry, University of Wisconsin, Madison, Wisconsin 53706, United States

[§]Department of Biological, Chemical and Physical Sciences, Roosevelt University, 430 South Michigan Avenue, Chicago, Illinois 60605, United States

Supporting Information

ABSTRACT: Superoxide dismutase (SOD) catalyzes the disproportionation of superoxide ($O_2^{\bullet -}$) into H_2O_2 and $O_2(g)$ by toggling through different oxidation states of a first-row transition metal ion at its active site. Ni-containing SODs (NiSODs) are a distinct class of this family of metalloenzymes due to the unusual coordination sphere that is comprised of mixed N/S-ligands from peptide-N and cysteine-S donor atoms. A central goal of our research is to understand the factors that govern reactive oxygen species (ROS) stability of the Ni−S(Cys) bond in NiSOD utilizing a synthetic model approach. In light of the reactivity of metal-coordinated thiolates to ROS, several hypotheses have been proffered and include the coordination of His1-Nδ to the Ni(II) and Ni(III) forms of NiSOD, as well as hydrogen bonding or full protonation of a coordinated S(Cys). In this work, we present NiSOD analogues of the general formula $[Ni(N_2S)(SR')]^-$, providing a variable location (SR′ = aryl thiolate) in the N_2S_2 basal plane coordination sphere where we have introduced *o*-amino and/or electron-withdrawing groups to intercept an oxidized Ni species. The synthesis, structure, and properties of the NiSOD model complexes $(Et_4N)[Ni(nmp)(SPh\text{-}o\text{-}NH_2)]$ (**2**), $(Et_4N)[Ni(nmp)(SPh\text{-}o\text{-}NH_2\text{-}p\text{-}CF_3)]$ (**3**), $(Et_4N)[Ni(nmp)(SPh\text{-}p\text{-}NH_2)]$ (**4**), and $(Et_4N)[Ni(nmp)(SPh\text{-}p\text{-}CF_3)]$ (**5**) (nmp^{2-} = dianion of *N*-(2-mercaptoethyl)picolinamide) are reported. NiSOD model complexes with amino groups positioned *ortho* to the aryl-S in SR′ (**2** and **3**) afford oxidized species ($\mathbf{2}^{ox}$ and $\mathbf{3}^{ox}$) that are best described as a resonance hybrid between Ni(III)-SR and Ni(II)-$^{\bullet}$SR based on ultraviolet−visible (UV-vis), magnetic circular dichroism (MCD), and electron paramagnetic resonance (EPR) spectroscopies, as well as density functional theory (DFT) calculations. The results presented here, demonstrating the high percentage of S(3*p*) character in the highest occupied molecular orbital (HOMO) of the four-coordinate reduced form of NiSOD ($NiSOD_{red}$), suggest that the transition from $NiSOD_{red}$ to the five-coordinate oxidized form of NiSOD ($NiSOD_{ox}$) may go through a four-coordinate Ni-$^{\bullet}$S(Cys) ($NiSOD_{ox}$-His_{off}) that is stabilized by coordination to Ni(II).

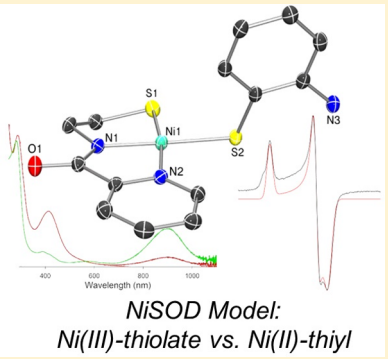

NiSOD Model: Ni(III)-thiolate vs. Ni(II)-thiyl

INTRODUCTION

Aerobic organisms utilize superoxide dismutase (SOD) metalloenzymes in their defense against the free radical superoxide ($O_2^{\bullet -}$), which if unregulated plays a role in a variety of disease states.[1−8] The most recently discovered class of SODs are the nickel-containing SODs (NiSODs), which utilize Ni in a mixed nitrogen and thiolate coordination environment to catalyze the disproportionation of $O_2^{\bullet -}$ to H_2O_2 and O_2 by cycling through Ni(II/III) redox states (see eqs 1 and 2 in Figure 1).[9] X-ray crystal structures of NiSOD from two separate *Streptomyces* strains confirm two distinct metal coordination geometries.[10−12] In the reduced form ($NiSOD_{red}$), the low-spin (S = 0) Ni(II) ion lies in a square-planar N_2S_2 environment composed of the N-terminal amine of His1, the deprotonated peptido-N of Cys2, and two thiolato-S from Cys2 and Cys6 (Figure 1). The oxidized form ($NiSOD_{ox}$) contains the same ligand set, but the $S = {}^1/_2$ Ni(III) ion is five-coordinate and additionally bound to the imidazole-Nδ of His1 resulting in a Ni−N_3S_2 square-pyramidal geometry (Figure 1).[10−12]

Questions concerning the enzyme's unusual N/S coordination sphere, particularly its stability toward O_2 and reactive oxygen species (ROS), in light of the reactive Ni−S(Cys) bonds,[13] and the catalytic mechanism have prompted researchers to develop maquette-based,[14−20] tripeptide,[21−24] and low molecular weight[25−38] analogues that seek to replicate NiSOD's structure and/or function.[39,40] Indeed, several experimental and theoretical efforts have suggested that the mixed peptide-N/amine-N ligation serves as one key factor to promote greater Ni-character in the redox-active molecular

Received: December 31, 2014
Published: April 2, 2015

DOI: 10.1021/ic503124f
Inorg. Chem. 2015, 54, 3815−3828

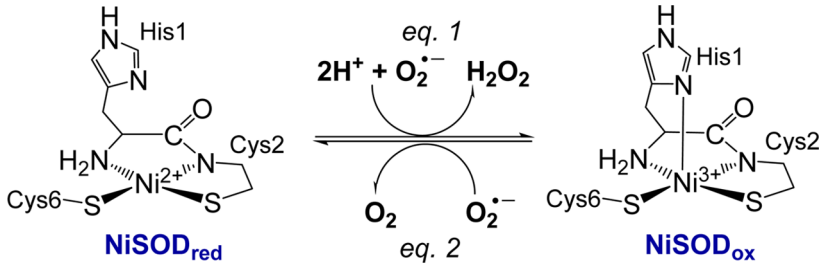

Figure 1. Structures of the NiSOD active site and the corresponding SOD half-reactions.

orbital of NiSOD, in particular for the Ni(II) or NiSOD$_{red}$ state, thus preventing unwanted S-oxidation/oxygenation.[10,30,41] For example, a direct electronic structure comparison of two planar Ni(II)-N_2S_2 complexes (NiSOD$_{red}$ models) with diamine/dithiolate versus amine/carboxamide/dithiolate donors revealed a significant increase in Ni character of the Ni($d\pi$)−S($p\pi$) antibonding highest occupied molecular orbital (HOMO) upon introduction of the carboxamide, i.e., 18% Ni, 74% S for diamine; 33% Ni, 50% S for amine/carboxamide.[30] Direct density functional theory (DFT) computations on truncated versions of NiSOD$_{red}$ clearly demonstrated more S($p\pi$) character than Ni($d\pi$) character in the π-antibonding HOMO (25% Ni, 67% S) and HOMO−1 (37% Ni, 44% S).[10] Taken together, these results support a highly covalent Ni−S bond in NiSOD$_{red}$ that, nonetheless, still has significant S-character in the HOMO even with inclusion of the Ni−N$_{peptide}$ bond. Thus, the enzyme has evolved in such a way to promote Ni-based oxidation via the destabilization of the Ni($d\pi$) orbitals. This proposal has been verified by examining the electronic structure of the DFT-generated hypothetical four-coordinate (4C) planar version of NiSOD$_{ox}$, namely NiSOD$_{ox}$-His$_{off}$, that revealed a HOMO composition of 58% Ni($d\pi$) and 24% S($p\pi$).[10] On the other hand, the actual NiSOD$_{ox}$ HOMO is predominantly Ni in character with the unpaired electron occupying the Ni d_{z^2} orbital, as verified by electron paramagnetic resonance (EPR) spectroscopy. Thus, the electronic structural changes from NiSOD$_{red}$ → NiSOD$_{ox}$-His$_{off}$ → NiSOD$_{ox}$ gradually move toward more Ni-character in the HOMO. This analysis begs the question as to what prevents NiSOD$_{red}$ from undergoing deleterious S-based redox chemistry upon conversion to NiSOD$_{ox}$. Could a Ni-stabilized $^{\bullet}$S(Cys) be traversed in such a conversion? To date, few low molecular weight analogues of NiSOD with mixed peptide-N/amine-N/thiolate-S coordination have been shown to achieve catalytic $O_2^{\bullet-}$ disproportionation. Many such complexes are prone to undergo irreversible S-based rather than Ni-based oxidation although in some cases, a transient Ni(III) species has been trapped and observed by EPR spectroscopy.[35,42,43]

The work presented here adopts the methodology developed by our group for synthesizing asymmetric, 4C planar Ni−N_2S_2 models of NiSOD employing the nmp^{2-} ligand (see Chart 1; nmp^{2-} = dianion of *N*-(2-mercaptoethyl)picolinamide).[32] Synthesis of such models was achieved through splitting of a proposed *S*,*S*-bridged dimer [$Ni_2(nmp)_2$] with exogenously added thiolate ions or S$_{exo}$ (where exo refers to the exogenously added monodentate S-ligand) that afforded a variety of Ni(II)-N_2S_2 complexes. We now report this *S*,*S*-bridged species to be the tetramer [$Ni_4(nmp)_4$] (**1**). The use of S$_{exo}$ to complete the N_2S_2 coordination sphere is synthetically novel in that it provides a specific point of control for modeling Cys6 (see Figure 1) at a site-differentiated location in the coordination sphere. In this way, the electronic properties of the complex can be evaluated and tuned by changing S$_{exo}$. Prior work on Ni(II)-nmp systems focused on synthetic methodology[32] and the electronic influence of second-sphere N−H···S hydrogen bonds (H-bonds).[33] None of these complexes afforded a stable oxidized species. Instead, oxidation took place at S$_{exo}$ to afford the disulfide of S$_{exo}$ (through a transient thiyl radical) and **1** in quantitative yields. We hypothesized that enforcing a potential N-donor near the Ni center and/or decreasing the basicity of S$_{exo}$ would allow us to intercept a Ni(III) or Ni(II)-thiyl species. Indeed, the presence of N$_{axial}$ ligands has proven beneficial in spectroscopically observing other Ni(III)-N_2S_2 complexes related to NiSOD.[36,44] Thus, the primary objective of this work is to gauge the impact of electronically deficient S$_{exo}$ and N$_{axial}$-tethered S$_{exo}$ donors on the redox properties of the corresponding NiSOD model complexes. The synthesis, structure, properties, and reactivity of the following Ni−N_2S_2 complexes will be described: (Et_4N)[Ni(nmp)(SPh-*o*-NH_2)] (**2**), (Et_4N)[Ni(nmp)(SPh-*o*-NH_2-*p*-CF_3)] (**3**), (Et_4N)[Ni(nmp)(SPh-*p*-NH_2)] (**4**), and (Et_4N)[Ni(nmp)(SPh-*p*-CF_3)] (**5**) (Chart 1). The NiSOD model complexes with amino groups positioned *ortho* to the aryl-S (**2** and **3**) afforded oxidized species that are best described as a resonance hybrid between Ni(III)-($^{-}$SR) and Ni(II)-($^{\bullet}$SR) and are the first examples of the room temperature (RT) observation of Ni-stabilized thiyl radicals with relatively long (hours) lifetimes.

Chart 1. General Structure of the [Ni(nmp)(SR)]$^-$ Complexes Reported in This Study[a]

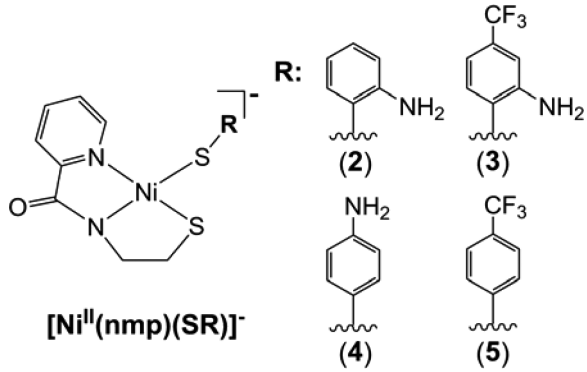

[a]R = 2-aminothiophenolate (**2**), 2-amino-4-(trifluoromethyl)-benzenethiolate (**3**), 4-aminothiophenolate (**4**), 4-(trifluoromethyl)-thiophenolate (**5**).

EXPERIMENTAL SECTION

General Information. All reagents were purchased from commercial sources and used as received, unless otherwise noted. Acetonitrile (MeCN), tetrahydrofuran (THF), diethyl ether (Et_2O), and pentane were purified by passage through activated alumina

DOI: 10.1021/ic503124f
Inorg. Chem. 2015, 54, 3815−3828

columns of an MBraun MB-SPS solvent purification system and stored under an N_2 atmosphere until use. *N,N*-dimethylformamide (DMF) was purified with a VAC solvent purifier containing 4 Å molecular sieves and stored under N_2. The ligand *N*-2-(mercaptoethyl)-picolinamide ($nmpH_2$; H represents dissociable protons) and its corresponding Ni(II) complex, $[Ni_4(nmp)_4]$ (**1**), were prepared according to the published procedure.[32] All reactions were performed under an inert atmosphere of N_2 using Schlenk line techniques or under an atmosphere of purified N_2 in an MBraun Unilab glovebox. The syntheses of Et_4N^+ thiolate salts from Et_4NCl and the appropriate sodium thiolate were carried out according to previously published methods.[45,46]

Physical Methods. Fourier transform infrared (FTIR) spectra were collected on a ThermoNicolet Model 6700 spectrophotometer running the OMNIC software. All samples were run as solid samples prepared as pressed KBr pellets. X-band (9.60 GHz) EPR spectra were obtained using a Bruker ESP 300E EPR spectrometer controlled with a Bruker microwave bridge at 10 K. The EPR was equipped with a continuous-flow liquid He cryostat and a temperature controller (ESR 9) made by Oxford Instruments, Inc. EPR spectra were simulated using the program QPOWA, as modified by J. Telser.[47] Electronic absorption spectra were collected at 298 K using a Varian Model Cary-50 spectrophotometer containing a Quantum Northwest TC 125 temperature control unit. The UV-vis samples were prepared in gas-tight Teflon-lined screw cap quartz cells with an optical path length of 1 cm. Cyclic voltammetry (CV) measurements were performed with a PAR Model 273A potentiostat using a Ag/Ag^+ (0.01 M $AgNO_3$/0.1 M $^nBu_4NPF_6$ electrolyte in MeCN) reference electrode, a Pt counter electrode, and a glassy carbon working milli-electrode (diameter = 2 mm). CV measurements were performed at ambient temperature using 3.5 or 8.0 mM analyte in DMF under Ar containing 0.1 M $^nBu_4NPF_6$ as the supporting electrolyte. The "maximize stability" mode and a low-pass 5.3 Hz filter were used in the PAR PowerCV software. Analyte potentials were referenced against a 0.05−0.1 mM ferrocene standard. ^1H NMR spectra were recorded in the listed deuterated solvent on a 400 MHz Bruker Model BZH 400/52 NMR spectrometer or a Varian Unity Inova 500 MHz NMR spectrometer at RT with chemical shifts internally referenced to tetramethylsilane (TMS = $Si(CH_3)_4$), or the residual protio signal of the deuterated solvent.[48] Low-resolution electrospray ionization mass spectrometry (LR-ESI-MS) data were collected using a Bruker Model Esquire 3000 plus ion-trap mass spectrometer. High-resolution electrospray ionization mass spectrometry (HR-ESI-MS) data were collected using an Orbitrap Elite system with precision to the third decimal place. Magnetic circular dichroism (MCD) and low temperature absorption data were collected using a Jasco Model J-715 spectropolarimeter, in conjunction with an Oxford Instrument SM-4000 8T magnetocryostat. The sample for these studies was prepared in a 1:4 (v/v) solvent mixture of MeCN and butyronitrile and sparged with dry $O_2(g)$ for 5 min. Glass strain contributions to the MCD signal were removed by taking the difference between spectra collected with the magnetic field aligned parallel and antiparallel to the light-propagation axis. Elemental analysis for C, H, and N was performed at QTI-Intertek in Whitehouse, NJ and ALS Environmental (formerly Columbia Analytical Services) in Tucson, AZ.

(Et_4N)[Ni(nmp)(SPh-*o*-NH_2)] (2). To a 6 mL DMF slurry of **1** (0.1550 g, 0.1622 mmol) was added a yellow DMF solution (2 mL) of (Et_4N)(SPh-*o*-NH_2) (0.1517 g, 0.5962 mmol) dropwise at RT. The DMF gradually took up a burgundy-red color over time. The mixture was stirred under N_2 for 20 h in a 40 °C water bath. The resulting dark red, mostly homogeneous solution was filtered through Celite to remove unreacted **1**, and the filtrate was evaporated to dryness via short-path vacuum distillation. The resulting brown-black residue was dissolved in 5 mL of MeCN, cooled to −20 °C, and filtered through a plug of Celite. The dark red MeCN filtrate was removed under vacuum, and the residue stirred in 5 mL of Et_2O overnight to afford 0.2093 g (0.3554 mmol, 60%) of an orange-red powder. ^1H NMR (500 MHz, $CDCl_3$ containing 0.05% v/v TMS, δ from TMS): 8.49 (d, 1H, J = 10.0 Hz), 8.13 (d, 1H, J = 10.0 Hz), 7.69 (m, 2H), 7.10 (t, 1H, J = 8.0 Hz), 6.75 (t, 1H, J = 9.3 Hz), 6.48 (m, 2H), 4.81 (s, 2H, NH_2), 3.45 (t, 2H, J = 6.5 Hz, $-NCH_2CH_2S-$), 3.22 (br, 9H integrates high due to the presence of excess Et_4N^+), 2.32 (t, 2H, J = 6.5 Hz, $-NCH_2CH_2S-$), 1.25 (br, 20H integrates high due to the presence of excess Et_4N^+). FTIR (KBr pellet) ν_{max} (cm^{-1}): 3407 (m, ν_{NH}), 3309 (m, ν_{NH}), 2974 (w), 2915 (w), 2846 (w), 1670 (m, ν_{CO} of residual DMF), 1617 (vs, ν_{CO}), 1593 (vs, ν_{CO}), 1568 (m), 1559 (m), 1475 (m), 1437 (w), 1391 (s), 1293 (w), 1172 (w), 1093 (s), 999 (m), 786 (w), 755 (m), 687 (w), 623 (w), 558 (w), 485 (w). UV-vis (MeCN, 298 K) λ_{max}, nm (ε, M^{-1} cm^{-1}): 453 (7200). LR-ESI-MS (m/z): $[M-Et_4N]^-$ calcd for $C_{14}H_{14}N_3OS_2Ni$, 362.0 (100.0), 364.0 (49.3), 363.0 (18.1), 365.0 (10.3), 366.0 (10.2); found: 361.9 (100.0), 363.9 (47.4), 362.9 (14.4), 364.9 (8.5), 365.8 (9.4). HR-ESI-MS (m/z): $[M-Et_4N]^-$ calcd for $C_{14}H_{14}N_3OS_2Ni$, 361.994 (100.0), 363.989 (47.6), 362.996 (15.2), 364.992 (7.2), 365.986 (5.4); found: 361.994 (100.0), 363.990 (48.9), 362.997 (15.0), 364.992 (6.9), 365.986 (8.1). Anal. Calcd for $C_{22}H_{34}N_4OS_2Ni{\cdot}H_2O{\cdot}MeCN{\cdot}0.5DMF$: C, 52.00; H, 7.27; N, 13.08. Found: C, 51.39; H, 6.56; N, 13.21.

(Et_4N)[Ni(nmp)(SPh-*o*-NH_2-*p*-CF_3)] (3). To a 6 mL DMF slurry of **1** (0.2380 g, 0.2490 mmol) was added a bright yellow DMF (3 mL) solution of (Et_4N)(SPh-*o*-NH_2-*p*-CF_3) (0.3012 g, 0.9342 mmol). The solvent gradually took up a reddish-brown color over time. The mixture was stirred under N_2 for 20 h in a 40 °C water bath. The resulting dark red, mostly homogeneous solution was filtered to remove unreacted **1**, and the filtrate was evaporated to dryness via short-path vacuum distillation. The resulting red-burgundy residue was dissolved in 5 mL of THF, cooled to −20 °C, and filtered through a plug of Celite. The dark red THF filtrate was removed under vacuum to result in a black oily material. This residue was triturated with 5 mL of Et_2O or pentane overnight to afford a burgundy-black powder (0.4150 g, 0.6935 mmol, 74%). ^1H NMR (500 MHz, CD_3CN, δ from protio solvent): 8.48 (d, 1H, J = 5.0 Hz), 8.11 (d, 1H, J = 10.0 Hz), 7.83 (t, 1H, J = 8.5 Hz), 7.51 (d, 1H, J = 10.0 Hz), 7.25 (t, 1H, J = 8.5 Hz), 6.69 (s, 1H), 6.60 (d, 1H, J = 10.0 Hz), 5.13 (s, 2H, NH_2), 3.22 (t, 2H, J = 6.5 Hz, $-NCH_2CH_2S-$), 3.15 (q, 23H, integrates high due to the presence of excess Et_4N^+, J = 10.0 Hz), 2.12 (t, 2H, J = 6.5 Hz, $-NCH_2CH_2S-$), 1.19 (t, 34H, integrates high due to the presence of excess Et_4N^+, J = 7.5 Hz). FTIR (KBr pellet) ν_{max} (cm^{-1}): 3407 (w,ν_{NH}), 3286 (w,ν_{NH}), 2980 (w), 2917 (w), 2849 (w), 1765 (w), 1620 (vs, ν_{CO}), 1592 (vs, ν_{CO}), 1483 (m), 1432 (m), 1329 (vs), 1102 (m), 1072 (m), 999 (w), 787 (w). UV-vis (MeCN, 298 K) λ_{max}, nm (ε, M^{-1} cm^{-1}): 448 (3800). LR-ESI-MS (m/z): $[M-Et_4N]^-$ calcd for $C_{15}H_{13}F_3N_3OS_2Ni$, 430.0 (100), 432.0 (49.5), 431.0 (19.1), 433.0 (10.8), 434.0 (10.3); found: 429.8 (100.0), 431.8 (48.0), 430.8 (16.1), 432.8 (9.1), 433.8 (8.8). HR-ESI-MS (m/z): $[M-Et_4N]^-$ calcd for $C_{15}H_{13}F_3N_3OS_2Ni$, 429.981 (100.0), 431.977 (47.6), 430.984 (16.2), 432.979 (6.2), 433.974 (5.3); found: 429.982 (100.0), 431.977 (47.2), 430.985 (16.9), 432.980 (8.1), 433.974 (8.1). Anal. Calcd for $C_{23}H_{33}F_3N_4OS_2Ni{\cdot}0.5Et_2O$: C, 50.18; H, 6.40; N, 9.36. Found: C, 50.10; H, 6.07; N, 9.09.

(Et_4N)[Ni(nmp)(SPh-*p*-NH_2)] (4). To a 6 mL DMF slurry of **1** (0.1783 g, 0.1866 mmol) was added a pale yellow DMF solution (2 mL) of (Et_4N)(SPh-*p*-NH_2) (0.1709 g, 0.6717 mmol) dropwise at RT. The DMF solvent gradually took up a burgundy-red color over time. The mixture was stirred under N_2 for 20 h in a 40 °C water bath. The resulting dark burgundy, mostly homogeneous solution was filtered through Celite to remove unreacted **1**, and the filtrate was evaporated to dryness via short-path vacuum distillation. The resulting brown-black residue was dissolved in 5 mL of MeCN, cooled to −20 °C, and filtered through Celite. The burgundy MeCN filtrate was removed under vacuum and the resulting black residue was stirred in 5 mL of Et_2O overnight to afford 0.1741 g (0.3138 mmol, 47%) of an orange-red powder. ^1H NMR (500 MHz, $CDCl_3$ containing 0.05% v/v TMS, δ from TMS): 8.60 (d, 1H, J = 10.0 Hz), 7.69 (m, 4H), 7.12 (t, 1H, J = 10.0 Hz), 6.41 (d, 2H, J = 10.0 Hz), 3.44 (t, 2H, J = 6.5 Hz, $-NCH_2CH_2S-$), 3.37 (s, 2H, NH_2), 3.31 (q, 10H, integrates high due to the presence of excess Et_4N^+, J = 10.0 Hz), 2.31 (t, 2H, J = 6.5, $-NCH_2CH_2S-$), 1.28 (t, 15H, integrates high due to the presence of excess Et_4N^+, J = 7.5 Hz). FTIR (KBr pellet) ν_{max} (cm^{-1}): 3315 (m,ν_{NH}), 3197 (m,ν_{NH}), 2983 (w), 2912 (w), 2841 (w), 1671 (m, ν_{CO} of residual DMF), 1616 (vs, ν_{CO}), 1592 (vs, ν_{CO}), 1486 (s), 1455 (m),

DOI: 10.1021/ic503124f
Inorg. Chem. 2015, 54, 3815−3828

1396 (m), 1268 (w), 1174 (w), 1096 (s), 1002 (w), 817 (w), 794 (w), 766 (w), 718 (w), 704 (w), 688 (w), 631 (w). UV-vis (MeCN, 298 K), λ_{max}, nm (ε, M^{-1} cm^{-1}): 458 (6100). LR-ESI-MS (m/z): $[M-Et_4N]^-$ calcd for $C_{14}H_{14}N_3OS_2Ni$, 362.0 (100.0), 364.0 (49.3), 363.0 (18.1), 365.0 (10.3), 366.0 (10.2); found: 361.9 (100.0), 363.9 (43.8), 362.9 (19.1), 364.9 (10.0), 365.9 (7.0). HR-ESI-MS (m/z): $[M-Et_4N]^-$ calcd for $C_{14}H_{14}N_3OS_2Ni$, 361.994 (100.0), 363.989 (47.6), 362.996 (15.2), 364.992 (7.2), 365.986 (5.4); found: 361.994 (100.0), 363.989 (47.3), 362.997 (15.5), 364.992 (6.5), 365.986 (8.0). Anal. Calcd for $C_{22}H_{34}N_4OS_2Ni{\cdot}H_2O{\cdot}0.5THF{\cdot}0.1DMF$: C, 52.61; H, 7.40; N, 10.35. Found: C, 52.74; H, 7.91; N, 10.37.

(Et_4N)[Ni(nmp)(SPh-*p*-CF_3)] (5). To a 6 mL DMF slurry of **1** (0.0849 g, 0.0888 mmol) was added a pink DMF solution of (Et_4N)(SPh-*p*-CF_3) (0.1023 g, 0.3328 mmol) dropwise at RT. The solvent gradually took up a burgundy-red color over time. The mixture was stirred under N_2 for 20 h in a 40 °C water bath. The resulting dark red, mostly homogeneous solution was filtered through Celite to remove unreacted **1**, and the filtrate was evaporated to dryness via short-path vacuum distillation. The resulting brown-black residue was dissolved in 5 mL of THF, cooled to −20 °C, and filtered through a plug of Celite. The dark red THF filtrate was removed under vacuum and the resulting dark black residue was stirred in 5 mL of Et_2O overnight to afford 0.0858 g (0.157 mmol, 47%) of a burgundy-black sticky material. ^1H NMR (400 MHz, CD_3CN, δ from protio solvent): 8.53 (d, 1H, J = 6.0 Hz), 8.09 (d, 2H, J = 8.4 Hz), 7.83 (t, 1H, J = 8.0 Hz), 7.52 (d, 1H, J = 7.6 Hz), 7.24 (t, 1H, J = 7.0 Hz), 7.17 (d, 2H, J = 8.0 Hz), 3.23 (t, 2H, J = 6.5 Hz, $-NCH_2CH_2S-$), 3.15 (q, 14H, integrates high due to the presence of excess Et_4N^+, J = 7.6 Hz), 2.16 (br, 4H, integrates high due to overlap with H_2O, $-NCH_2CH_2S-$), 1.19 (t, 20H, integrates high due to the presence of excess Et_4N^+, J = 8.0 Hz). FTIR (KBr pellet) ν_{max} (cm^{-1}): 2981 (w), 2914 (w), 2839 (w), 1670 (s, ν_{CO} of residual DMF), 1623 (vs, ν_{CO}), 1593 (vs, ν_{CO}), 1560 (m), 1486 (m), 1458 (w), 1385 (s), 1323 (s), 1274 (w), 1256 (w), 1183 (w), 1155 (w), 1086 (s), 1058 (m), 1009 (w), 826 (w), 761 (w), 686 (w). UV-vis (MeCN, 298 K), λ_{max}, nm (ε, M^{-1} cm^{-1}): 432 (4600). LR-ESI-MS (m/z): $[M-Et_4N]^-$ calcd for $C_{15}H_{12}F_3N_2OS_2Ni$, 415.0 (100.0), 417.0 (49.4), 416.0 (18.7), 418.0 (10.6), 419.0 (10.3); found: 414.8 (100.0), 416.8 (48.0), 415.8 (16.8), 417.8 (8.5), 418.7 (8.9). HR-ESI-MS measured with Na^+ salt (m/z): calcd for $C_{15}H_{12}F_3N_2OS_2Ni$, 414.970 (100.0), 416.966 (47.6), 415.973 (16.2), 417.968 (6.2), 418.963 (5.3); found: 414.970 (100.0), 416.965 (47.3), 415.973 (15.8), 417.968 (7.1), 418.962 (8.1). Anal. Calcd for $C_{23}H_{32}F_3N_3OS_2Ni$: C, 50.56; H, 5.90; N, 7.69. Found: C, 49.41; H, 5.99; N, 6.29. A reasonable fit to C, H, N could not be obtained due to the oily nature of the resulting product.

X-ray Crystallographic Data Collection and Structure Solution and Refinement. Red needlelike crystals of **1** were grown by Et_2O layering over a CD_3OD solution of Na_3[{Ni(nmp)}$_3$(BTAS)] ($BTAS^{3-}$ is the trianion of N^1,N^3,N^5-tris(2-mercaptoethyl)benzene-1,3,5-tricarboxamide) at RT under aerobic atmosphere. Dark red bladelike crystals of **2** were grown by slow vapor diffusion of Et_2O into a solution of **2** in DMF:C_6H_5Cl (1:1) at RT. In addition, dark red blade crystals of **4** were grown by slow vapor diffusion of Et_2O into a solution of **4** in THF:DMF (~4:1) at RT. Suitable crystals were mounted on a glass fiber. The X-ray intensity data were measured at 100 K on a Bruker SMART APEX II X-ray diffractometer system with graphite-monochromatic Mo Kα radiation (λ = 0.71073 Å), using ω-scan technique controlled by the SMART software package.[49] The data were corrected for Lorentz and polarization effects[50] and integrated with the manufacturer's SAINT software. Absorption corrections were applied with the program SADABS.[51] Subsequent structure refinement was performed using the SHELXTL 6.1 solution package operating on a Pentium computer. The structure was solved by direct methods using the SHELXTL 6.1 software package.[52,53] All non-hydrogen atoms were refined anisotropically.[54] Non-hydrogen atoms were located from successive difference Fourier map calculations. In the structure of **1**, two carbon atoms (C1 and C2) and one oxygen atom (O1) were found disordered in two sets of each: labeled for the carbon atoms as C1 and C2 (one set) and C1′ and C2′ (other set); and labeled for the oxygen atom as O1 (one set) and O1′ (other set), respectively. The two sets for the atoms (C1 and C2) were divided using the PART commands and proper restraints. The set of C1 and C2 has 46% occupancy while the other (C1′ and C2′) has 54% occupancy. The occupancies for O1 and O1′ are set at 50% each. The structure of **4** has two distinct, but chemically indistinguishable Ni complexes. Selected data and metric parameters for complexes **1**, **2**, and **4** are summarized in Table S1 in the Supporting Information and Table 1, respectively. Perspective views of the complexes were obtained using ORTEP.[55]

Table 1. Selected Bond Distances (Å) and Bond Angles (deg) for $[Ni_4(nmp)_4]$ (1), (Et_4N)[Ni(nmp)(SPh-*o*-NH_2)] (2), and (Et_4N)[Ni(nmp)(SPh-*p*-NH_2)] (4)

	1	2	4[a]
Bond Lengths (Å)			
Ni(1)−N(1)	1.866(4)	1.8750(16)	1.8698(14)
Ni(1)−N(2)	1.951(4)	1.9418(16)	1.9450(14)
Ni(1)−S(1)	2.1500(12)	2.1386(6)	2.1474(5)
Ni(1)−S(2)	2.2170(12)	2.2173(6)	2.2160(5)
Bond Angles (deg)			
N(1)−Ni(1)−N(2)	83.47(16)	83.36(7)	83.12(6)
N(1)−Ni(1)−S(1)	87.33(12)	88.62(5)	87.88(4)
N(1)−Ni(1)−S(2)	178.39(14)	178.74(5)	177.51(4)
N(2)−Ni(1)−S(1)	168.73(12)	171.97(5)	168.97(4)
N(2)−Ni(1)−S(2)	95.78(11)	97.60(5)	99.36(4)
S(1)−Ni(1)−S(2)	93.25(5)	90.41(2)	89.621(18)
C(9)−S(2)−Ni(1)	108.44(17)	104.66(6)	107.39(6)

[a]Parameters for one of the two unique, but chemically similar, Ni complexes observed in the asymmetric unit of **4**.

Computations. All computations were performed using the ORCA 2.9.0 program developed by Dr. Frank Neese.[56] The crystallographically determined coordinates for **2** provided the initial structures for the computational model (**II**) and its one-electron oxidized derivative (**II^{ox}**). Both models were then subjected to unconstrained geometry optimizations within the framework of DFT using Becke's three-parameter hybrid functional and the Lee−Yang−Parr correlation functional (B3LYP).[57,58] Ahlrichs' valence triple-ζ basis set, TZV(P) basis set,[59,60] was chosen for the Ni, N, and S atoms, respectively, while Ahlrichs' polarized split valence and auxiliary basis sets,[59] SV(P) and SV/C, were selected for all of the remaining atoms. The spin-restricted formalism was chosen for **II**, while the spin-unrestricted formalism was used for **II^{ox}**, which was modeled as $S = {}^1/_2$. Single-point DFT calculations on the geometry-optimized models were performed using the same functional and basis sets as those used in the geometry optimizations. The Pymol program[61] was utilized to generate isosurface plots of MOs and spin densities with isodensity values of 0.05 and 0.005 a.u., respectively.

The ORCA 2.9.0 program was also employed to compute EPR parameters for the geometry-optimized model **II^{ox}** by using the DFT-based coupled-perturbed self-consistent field approach in conjunction with the B3LYP functional. This calculation was performed using the CP(PPP) basis set[62,63] for Ni, Kutzelnigg's NMR/EPR (IGLO-III) basis set[64] for all N and S atoms, and the TZV(P) basis set for the remaining atoms.

Oxidation of 3. To a solution of **3** containing 10.9 mg of **3** (0.0194 mmol) stirring in 4 mL of DMF was added ceric ammonium nitrate (CAN) dropwise (1.748 mL of a 10.0 mM DMF solution, 0.0175 mmol) at RT. Upon the addition of CAN, the red-brown color associated with the Ni(II)-N_2S_2 complex was replaced by a dark-green color. The mixture was stirred for another 15 min at RT and filtered through a 0.2 μm nylon filter to yield a green transparent DMF solution. A red solid of a color consistent with a minor amount of **1** was evident in the filter. The oxidation was monitored by UV-vis and EPR spectroscopy.

DOI: 10.1021/ic503124f
Inorg. Chem. 2015, 54, 3815−3828

Oxidation of 2. Chemical oxidation of **2** was performed in the same manner as with **3**, except for using 11.2 mg (0.0227 mmol) of **2** and 2.045 mL of CAN (10.0 mM DMF solution, 0.0205 mmol). The red solution of **2** darkened to green upon the addition of CAN. Within minutes, the green color paled with the appearance of a red precipitate.

Oxidation of 4. Chemical oxidation of **4** was performed in the same manner as with **3**, except for using 9.6 mg (0.020 mmol) of **4** and 1.752 mL of CAN (10.0 mM DMF solution, 0.0175 mmol). The orange-red solution of **4** paled to light orange upon addition of CAN with the appearance of a red precipitate.

Oxidation of 5. Chemical oxidation of **5** was performed in the same manner as with **3**, except for using 8.9 mg (0.016 mmol) of **5** and 1.459 mL of CAN (10.0 mM DMF solution, 0.0146 mmol). The orange-red solution of **5** paled to light orange upon addition of CAN with the appearance of a red precipitate.

Reactivity. *UV-vis Monitoring of **3** and **3**^{ox} with NaN_3 and N-methylimidazole.* To a 5 mM DMF stock (2.5 mL) of **3** was added 10 equiv of *N*-methylimidazole (N-MeIm) or NaN_3, and the UV-vis spectrum was recorded. Solutions were oxidized in the same manner as above in the presence of 10 equiv of N-MeIm or NaN_3 to observe any changes in the electronic absorbance profile to indicate anion binding to the metal center.

Reactivity with KO_2. To 5 mM DMF solutions of **3** or **3**^{ox} (generated by adding 1 equiv of CAN to **3**) was added 1 equiv of KO_2 in DMF containing 18-crown-6 ether (4.1 equiv).[65] Workup of the reaction is as stated in Chart S2 in the SI.

RESULTS AND DISCUSSION

Synthesis. In previous work,[32,33] an *S*,*S*-bridged Ni-nmp unit was used as a metallosynthon to generate 4C planar Ni(II)-N_2S_2 complexes of the general formula $[Ni(nmp)(SR)]^-$ as active site models of $NiSOD_{red}$. The ligand nmp^{2-} is a tridentate chelate that contains pyridine-N, carboxamide-N, and alkyl thiolate-S donors that replicate the asymmetric ligand environment derived from His1 and Cys2 in the enzyme. In these reports, various ways of changing R on the monodentate thiolate (analogous to Cys6) were explored, and most syntheses were based on splitting a putative $[Ni_2(nmp)_2]$ *S*,*S*-bridged dimeric complex with various exogenous thiolate ligands. Elemental analysis and FTIR data of the solid were consistent with the proposed formula, but the poor solubility of this complex precluded more detailed spectroscopic and structural analyses. Based on a structure reported herein (vide infra), we describe this complex to be a tetrameric *S*,*S*-bridged species $[Ni_4(nmp)_4]$ (**1**) (Figure 2). While this result alters our prior synthetic schemes, it does not change the ratio of exogenous thiolate-to-Ni(nmp) used, i.e., 1:1 when considering single Ni(nmp) units in the *S*,*S*-bridged complex. As such, complexes **2**−**5** were synthesized by reacting a 40 °C DMF slurry of **1** with 4 equiv of the Et_4N^+ salts of various thiolates to yield the monomeric Ni(II) complexes in modest-to-good yields (50%−75%) (see Scheme 1). All complexes were isolated as analytically pure (except **5**) dark-red to orange-red solids of moderate stability to air. However, decomposition to the free thiol and **1** occurred when dissolved in protic solvents such as MeOH or H_2O, even under anaerobic conditions.

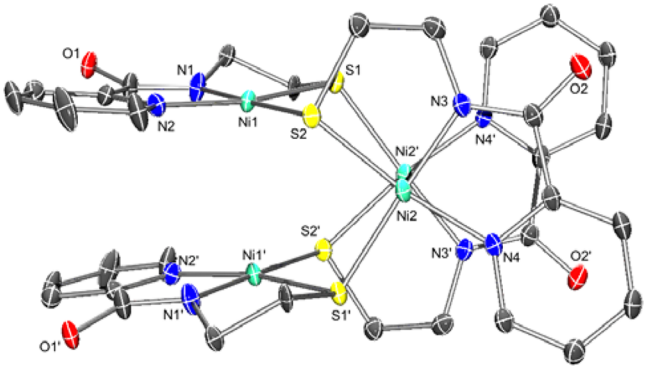

Figure 2. ORTEP of $[Ni_4(nmp)_4]$ (**1**) with the atom labeling scheme at 50% thermal probability. H atoms are omitted for clarity.

Scheme 1. Synthesis of Ni(II) Complexes[a]

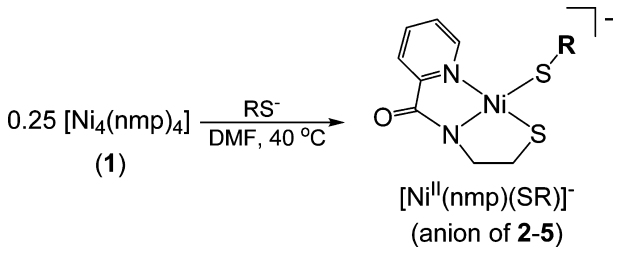

[a]R = SPh-*o*-NH_2 (**2**), SPh-*o*-NH_2-*p*-CF_3 (**3**), SPh-*p*-NH_2 (**4**), and SPh-*p*-CF_3 (**5**).

Spectroscopic Properties. Complexes **2**−**5** are soluble in polar solvents such as DMF and MeCN to form deeply colored red-brown solutions arising from charge-transfer (CT) bands in the 430−460 nm range (ε = 3800−7200 M^{-1} cm^{-1} in MeCN at 298 K). $NiSOD_{red}$ displays an absorption profile with a λ_{max} at 450 nm (ε = 480 M^{-1} cm^{-1}) and a shoulder at 543 nm (ε = 150 M^{-1} cm^{-1}) arising from *d*−*d* transitions,[10] a spectroscopic benchmark of 4C planar Ni(II) centers in an N_2S_2 coordination environment.[40] These ligand-field bands are masked in **2**−**5** by the intense CT features that involve electronic transitions between py-N and Ni(II).[33] Further solution measurements such as ^1H NMR experiments revealed that all complexes are diamagnetic, as expected for a 4C planar Ni(II) ion (see Figures S5, S7, S9, and S11 in the Supporting Information (SI)). These results do not exclude higher coordination numbers, as low-spin tbp or square-pyramidal Ni(II) would also be S = 0, but NMR results of known *o*-aminothiophenolate N,S-coordinated planar Ni(II) complexes exhibit shifts in the N*H*$_2$ resonance (δ_{NH_2}) by +1.4 ppm upon coordination.[66] In addition, the symmetric and asymmetric N−H stretches (ν_{NH}) of the NH_2 group red-shift by ∼200 cm^{-1} upon coordination.[66] The NH_2 proton resonance is close (+0.15−0.28 ppm) to the value obtained for the free thiolate and there are no significant changes in ν_{NH} in **2**−**4**. These minor changes in δ_{NH_2} and ν_{NH} confirm that no Ni(II)−NH_2Ph bond exists in **2**−**4** under the conditions used.

Structural Characterization. The tetrameric complex **1** and monomeric complexes **2** and **4** have been characterized by X-ray diffraction (XRD), the details of which can be found in the Experimental Section, Table 1, and Table S1 in the SI. Complex **1** crystallizes with four separate Ni(nmp) fragments bridged by the alkyl-S of another Ni(nmp) complex (see Figure 2). A summation of the significant bond lengths and angles is provided in Table 1, and a comparison with other monomeric $[Ni(nmp)(SR)]^-$ complexes is provided in Table 2. The tetramer is formed through specific Ni−S−Ni linkages (e.g., Ni1−S2−Ni2−S1′), such that each nmp-S bridges a different 4C planar Ni(II) ion. Compared to other reported $[Ni(nmp)(SR)]^-$ structures with NiN_2S_2 coordination,[32,33] the average Ni−$N_{carboxamide}$ distance (1.862 Å) is significantly shorter than

DOI: 10.1021/ic503124f
Inorg. Chem. 2015, 54, 3815−3828

Table 2. Selected Bond Distances for [Ni(nmp)(SR)]$^-$ NiSOD Model Complexes[a]

	Bond Distances (Å)			
R	Ni−$N_{carboxamide}$	Ni−N_{py}	Ni−S_{nmp}	Ni−S_{exo}
SPh-*p*-Cl	1.8638(14)	1.9470(14)	2.1492(5)	2.2139(4)
S^{t}Bu	1.882(2)	1.9635(19)	2.1629(7)	2.1938(7)
S-*o*-babt[b]	1.877(3)	1.947(3)	2.1518(12)	2.1939(14)
S-meb[c]	1.863(7)	1.944(7)	2.156(3)	2.172(3)
SPh-*o*-NH_2	1.8750(16)	1.9418(16)	2.1386(6)	2.2173(6)
SPh-*p*-NH_2	1.8698(14)	1.9450(14)	2.1474(5)	2.2160(5)
average	1.872 ± 0.008	1.948 ± 0.008	2.151 ± 0.008	2.201 ± 0.018

[a]Bond distances reported for Ni(1), N(1), N(2), S(1), and S(2) of the unit cell. [b]S-*o*-babt = anion of *o*-benzoylaminobenzenethiol. [c]S-meb = anion of *N*-(2-mercaptoethyl)benzamide.

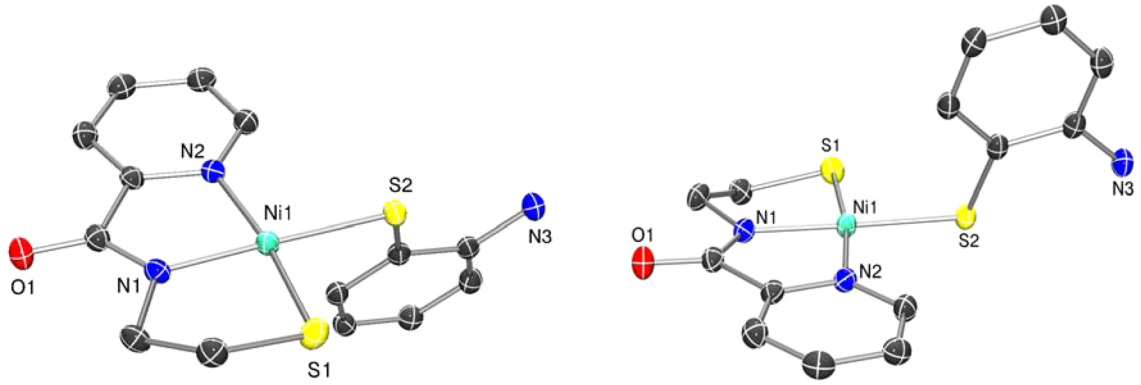

Figure 3. Different views of the ORTEP of the anion of (Et_4N)[Ni(nmp)(SPh-*o*-NH_2)] (**2**) with the atom labeling scheme at 50% thermal probability. H atoms are omitted for clarity.

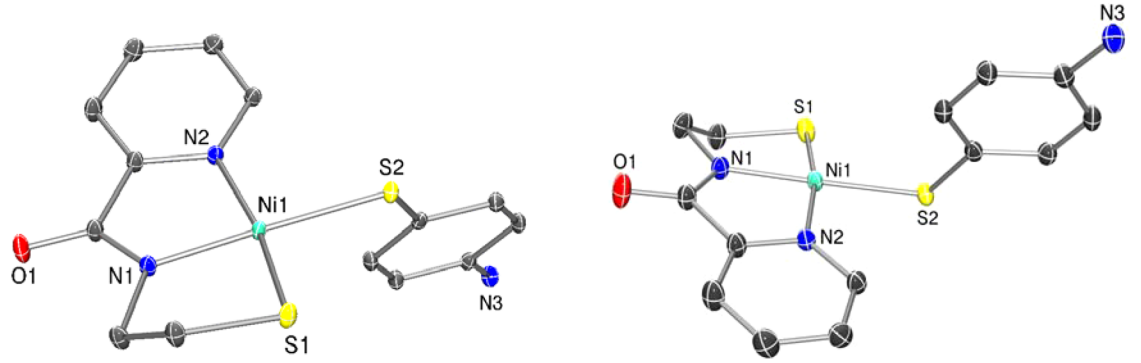

Figure 4. Different views of the ORTEP of the anion of (Et_4N)[Ni(nmp)(SPh-*p*-NH_2)] (**4**) with the atom labeling scheme at 50% thermal probability. H atoms are omitted for clarity.

that for Ni−N_{py} (1.943 Å), because of strong σ-donation by the carboxamide ligand. This property, along with the monodentate nature of SR, generally results in a longer Ni−S_{exo} versus Ni−S_{nmp} bond distance. Indeed, this bond is considerably longer in **1** (2.208 Å) than the Ni−S bond originating from the coordinated nmp^{2-} ligand (2.155 Å). In this case, S_{exo} represents a metallothiolate from another Ni(nmp) unit instead of an exogenously added thiolate ligand in prior reports. The average Ni···Ni separation is 3.4 Å, which precludes any direct Ni−Ni interaction.

Analogous to previously published [Ni(nmp)(SR)]$^-$ structures,[32,33] **2** and **4** (Figures 3 and 4, respectively and Figure S1 in the SI) demonstrated distorted 4C planar Ni(II) centers with two N- and two S-ligands in a *cis* disposition, resulting in a Ni(II)-N_2S_2 coordination sphere as in $NiSOD_{red}$. Crystallographic details and selected bond distances and angles are presented in Tables 1 and 2. Complex **4** crystallizes with two unique, but chemically equivalent, Ni(II)-N_2S_2 complexes. Bond distances are comparable to **1** and other [Ni(nmp)(SR)]$^-$ structures (Ni−$N_{carboxamide}$: 1.8750 Å (**2**), 1.8698 Å (**4**); Ni−N_{py}: 1.9418 Å (**2**), 1.9450 Å (**4**); Ni−S_{nmp}: 2.1386 Å (**2**), 2.1474 Å (**4**); Ni−S_{exo}: 2.2173 Å (**2**), 2.2160 Å (**4**); see Table 2 for a comparison with all structurally characterized Ni-nmp complexes) and reflect a trend in the electronic nature or Lewis basicity of the differing donor atoms. To emphasize the strong-field nature of the carboxamide donor, other 4C planar $NiSOD_{red}$ models (N = 4)[29,31,35,43] with multidentate chelates exhibit short Ni−$N_{carboxamide}$ bonds (average: 1.861 Å) and long Ni−$S_{trans\text{-}carboxamide}$ bonds (average: 2.175 Å) in their crystal structures. Thus, the lengthening of the Ni−S_{exo} bonds in **2** and

DOI: 10.1021/ic503124f
Inorg. Chem. 2015, 54, 3815−3828

4 is not solely due to the monodentate S_{exo} coordination. $NiSOD_{red}$ exhibits similar distances (average from the two reported *Streptomyces* structures): Ni-NH_2(His1): 1.97 ± 0.14 Å; Ni−$N_{peptide}$(Cys2): 1.93 ± 0.02 Å; Ni−S(Cys2): 2.20 ± 0.06 Å; Ni−S(Cys6- *trans* to peptide-N): 2.19 ± 0.01 Å.[11,12] The trends expected for the different Ni−N and Ni−S bonds are presumably muted in the enzyme structures due to poor resolution and the redox heterogeneity in the crystals (equal mix of Ni(II) and Ni(III) ions). In **2** and **4**, the closest Ni−NH_2 distance is 4.4 Å, establishing the absence of any five-coordinate species in the solid state. The Ni···N_{His} distance is also long in $NiSOD_{red}$, 4.26 Å (PDB: 1T6U) and 3.81 Å (PDB: 1Q0D), indicative of the nonbonding nature of this potential N-donor in the enzyme. Because of the *ortho*-positioning of the aniline-NH_2 in **2**, the N and coordinated S_{exo} are separated by 3.024 Å (sum of the van der Waals radii for N and S is 3.55 Å), which would suggest an intramolecular hydrogen bond with the ligated S. However, the N−H−S angle is estimated to be 110° (if H is placed in an ideal position), suggesting relatively poor orbital overlap between the donor−acceptor pair. Strong hydrogen bonds are usually linear in nature, i.e., ∠N−H···S ≈ 180°.[67] To emphasize the importance of this angle, hydrogen bonding to coordinated S-ligands in other NiSOD model compounds usually results in a decrease by 0.02−0.03 Å in the Ni−S distance due to relief of the Ni(dπ)−S(pπ) antibonding interaction, as the S lone pair is engaged in the hydrogen bond.[33,41] No such contraction of the Ni−S bonds was observed, when compared to the non-hydrogen-bonded complex **4**. Collectively analyzing the six structurally characterized complexes in this family (Table 2) revealed that distances to the nmp^{2-} ligating atoms are largely invariable. The largest variations appear in S_{exo} (Ni−S(avg.): 2.201 ± 0.018 Å), which range from 2.172 to 2.217 Å and generally correlate with the electronic nature of this particular S-donor.

Electrochemistry. To assess the role of the *o*-NH_2 group in the electrochemical activity of the Ni-nmp complexes, we performed cyclic voltammetry (CV) on **2**−**5**. Previously reported $[Ni^{II}(nmp)(SR)]^-$ complexes display irreversible waves in their CVs with cathodic and anodic peaks assigned to redox activity associated with the coordinated RS^- ligand, i.e., $[Ni^{II}(nmp)(SR)]^- \rightarrow 0.25[Ni^{II}_4(nmp)_4]$ (**1**) + 0.5RSSR.[32,33] Similar CVs and redox assignments were also observed with the peptide-based $[Ni^{II}$(GC-OMe)(SR)$]^-$ (GC-OMe is the dianion of H_2N-Gly-L-Cys-OMe) complexes.[34] In both cases, R represented simple aryl/alkyl thiolates or more complex thiolates with appended hydrogen-bonding moieties. In this study, we anticipated that providing a potential N-donor ligand from the *o*-aminothiophenolate would provide a viable mechanism to capture an oxidized species related to $NiSOD_{ox}$.

Representative CVs are displayed in Figures 5 and 6, as well as Figures S2 and S3 in the SI. All CVs were recorded in DMF at RT and *E* values are reported versus an externally referenced ferrocene/ferrocenium (Fc/Fc^+) couple using a glassy carbon working electrode and 0.1 M $^nBu_4NPF_6$ as the supporting electrolyte. Electrochemical measurements on **4** and **5**, complexes without an *o*-NH_2 group, revealed irreversible waves ($\Delta E_p \approx 1.5$ V) in the CV that are due to S_{exo} redox. The CV of **5** (containing the *p*-CF_3 group), for example, displayed two distinct electrochemical events at potentials of −1.64 V (E_{red}) and −0.19 V (E_{ox}) (Figure 5) that we assign as the $RS^\bullet$ (or 0.5 RSSR) → RS^- and RS^- → $RS^\bullet$ (or 0.5 RSSR) electrochemical reactions, respectively. These values are on par with reported potentials for simple organic disulfides such as

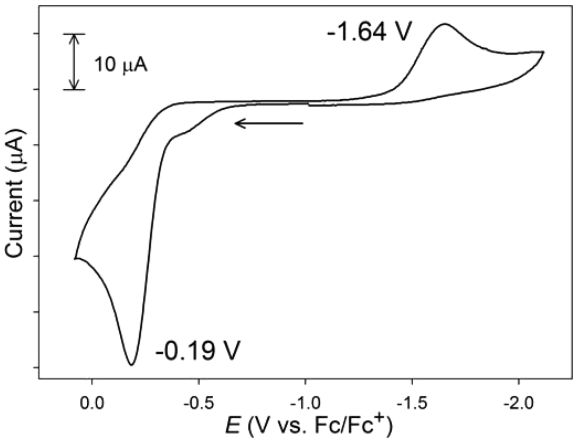

Figure 5. CV of an 8 mM solution of **5** in DMF at RT (glassy carbon working electrode, 0.1 M $^nBu_4NPF_6$ as the supporting electrolyte, 100 mV/s scan speed). The arrow shows the direction of the scan.

PhSSPh (E_{ox} = −0.49, E_{red} = −2.12 V vs Fc/Fc^+ in DMF)[68] and even more structurally complex thiolates that display qualitatively similar CVs.[69] The CV of a related 4C planar Ni(II)-NS_3 complex, $[Ni(pdmt)(SPh)]^-$ (pdmt = pyridine-2,6-dimethanethiolate), which also owes its electrochemical activity to the monodentate thiolate PhS^-, resembles the CV of **5** with values (E_{ox} = −0.47, E_{red} = −1.73 V in DMF) shifted approximately +0.20 V from that of free PhSSPh (above) due to coordination to Ni(II).[70] The comparative positive shift of ∼0.40 V in the $E_{red/ox}$ associated with **5** from PhSSPh is consistent with the electron-withdrawing *p*-CF_3 substituted aryl thiolate ligand. Complex **4** with the *p*-NH_2 substitution on SR behaved similarly (E_{ox} = −0.51 V in DMF) with additional low current intensity waves that we have yet to identify (see Figure S2 in the SI). Again, comparison with *p*-NH_2-PhSSPh-*p*-NH_2 (E_{ox} = −0.88, E_{red} = −2.33 V vs Fc/Fc^+ in DMF)[68] revealed a slight shift upon coordination of the thiolate to Ni(II). Regardless, the CVs of **4** and **5** only reflect ligand-based electrochemistry with no indication of a Ni(III/II) process. Additional verification of the reactions displayed in Scheme 2 (left side) comes from bulk oxidation experiments with CAN or Fc^+, which yielded **1** and the corresponding disulfide in near stoichiometric yield. Collectively, the $[Ni^{II}(nmp)(SR)]^-$ complexes with simple alkyl/aryl R-groups do not go through any observable Ni(III) state, as all oxidation chemistry is associated with S_{exo} (even the electron-deficient S_{exo} in **5**) and is suggestive of the high S-character in the HOMO of these complexes.

The CVs of **2** and **3** displayed similar irreversible waves with the exception of a quasi-reversible wave observed at $E_{1/2}$ = −0.69 V and −0.43 V for **2** and **3**, respectively (DMF, RT), that was slightly superimposed on E_{ox}. As expected, the oxidation of **2** is easier than **3** due to the *p*-CF_3 substitution on S_{exo}. Since the free *o*-aminothiophenolate is irreversibly oxidized at more positive potentials, this $E_{1/2}$ may be assigned as a metal-centered Ni(III/II) electron-transfer process. For simplicity, we will limit our discussion to complex **3**, but similar CVs were observed for **2** (see Figure S3 in the SI). The possibility of isolating and characterizing an oxidized NiSOD model, as suggested by the electrochemistry, led us to generate this species (termed $\mathbf{3^{ox}}$) by chemical oxidation with CAN and to study its redox properties. Interestingly, the CV of *in situ*-generated $\mathbf{3^{ox}}$ displayed a redox-couple at $E_{1/2}$ = −0.43 V (ΔE_p

DOI: 10.1021/ic503124f
Inorg. Chem. 2015, 54, 3815−3828

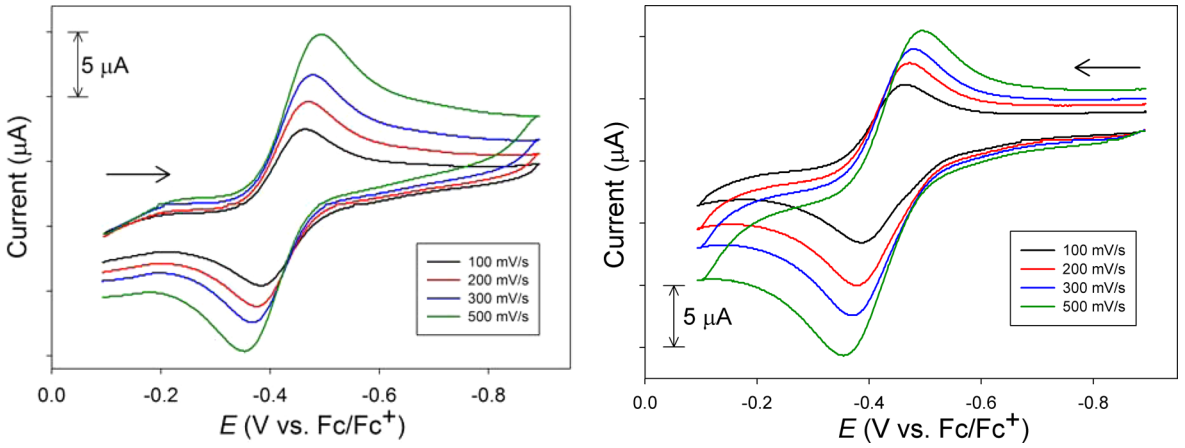

Figure 6. CV of a 3.5 mM solution of $\mathbf{3}^{ox}$ in DMF at RT from different scan directions (see arrow, glassy carbon working electrode, 0.1 M $^{n}Bu_4NPF_6$ as the supporting electrolyte).

Scheme 2. General Redox Activity of $[Ni(nmp)(SR)]^-$ Complexes

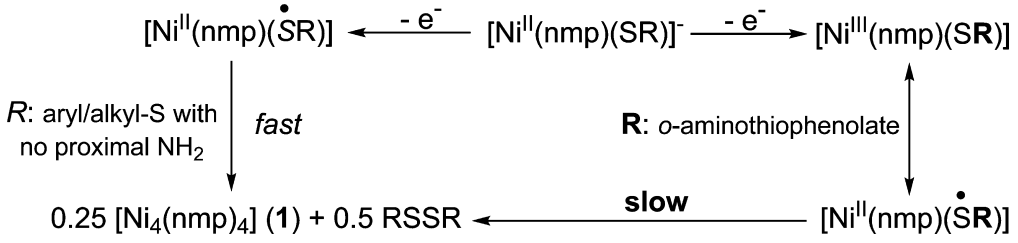

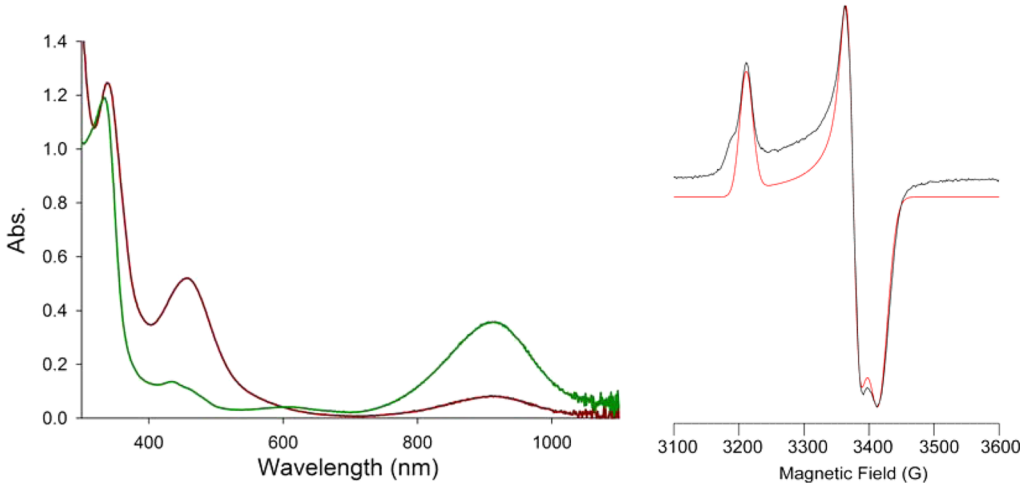

Figure 7. (Left) UV-vis spectrum of **3** (red trace) and *in situ*-generated $\mathbf{3}^{ox}$ (green trace) by addition of CAN to **3** in DMF at 298 K. (Right) X-band EPR spectrum (black trace) and simulation (red trace) of in situ generated $\mathbf{3}^{ox}$ in DMF at 10 K. Simulation parameters: g = [2.132, 2.028, 2.004], W = 35, 30, 45 MHz.

≈ 0.060 V; and i_{pa}/i_{pac} ≈ 1) that was remarkably similar to the CV of **3** (Figure 6 and Figure S3 in the SI). Additional metrics such as the linear (r^2 = 0.991, of $\mathbf{3}^{ox}$) i_p vs $\nu^{1/2}$ plot support the fact that this couple is a reversible, diffusion-controlled process. Scanning from either side of the isolated $E_{1/2}$ does not result in any changes (Figure 6). It is important to reiterate that $[Ni^{II}(nmp)(SR)]^-$ complexes do not exhibit any reversibility in their CVs (see Figure 5). The appearance of such a wave in the CV of **3** is thus a new feature in these otherwise isostructural NiSOD model complexes. A unique feature of **3** is the presence of the *o*-NH_2 group that must be the stabilizing feature to allow observation of such an oxidized species on the CV time scale. We propose that this redox event is due to one of the following couples: (i) $[Ni^{II}(nmp)(SR)]^-/[Ni^{III}(nmp)(SR)]$ or (ii) $[Ni^{II}(nmp)(SR)]^-/[Ni^{II}(nmp)(^{\bullet}SR)]$. In case (ii), the *o*-$NH_2$ group supports a coordinated S-radical to prevent the formation of RSSR and **1** that would result in the typical irreversible CVs (Scheme 2). Of course, a resonance description of $[Ni^{III}(nmp)(SR)] \leftrightarrow [Ni^{II}(nmp)(^{\bullet}SR)]$ is the more-realistic possibility (vide infra) (Scheme 2, right side).

Properties of $\mathbf{3}^{ox}$. Exposure of DMF solutions of **2** or **3** to air or $O_2(g)$ resulted in an immediate color change of the solution from red to green accompanied by the eventual formation of a red precipitate. These solutions afforded a broad, low-energy feature at ~900 nm in the RT electronic absorption spectrum. This transformation occurs on the minute (**2**, full

DOI: 10.1021/ic503124f
Inorg. Chem. 2015, 54, 3815−3828

formation of **1** within minutes) or hour (**3**, ~70% **1** after 24 h) time scale with the red precipitate confirmed to be **1**, suggesting the same ultimate fate as seen with other $[Ni(nmp)(SR)]^-$ complexes (Scheme 2). However, the difference here is that transient oxidized complexes are spectroscopically observable. Furthermore, chemical reduction of *in situ*-generated $\mathbf{3}^{ox}$ with $[Co(Cp)_2]$ resulted in regeneration of the reduced species **3** as verified by UV-vis, ^{1}H NMR, and ESI-MS experiments. Thus, bulk chemical oxidation and reduction mirrored the electrochemical observations and was also a reversible process. Due to the longer lifetime of $\mathbf{3}^{ox}$, we limit our discussion below to this species, although similar spectroscopic observations were noted for **2**.

To better identify the oxidized complex, we performed *in situ* spectroscopic characterization of the reaction mixture after chemically oxidizing **3** with oxidants such as CAN or Fc^+ salts. For example, addition of a stoichiometric amount of CAN to a DMF solution of **3** at RT immediately generated a green solution with a broad and intense absorption band at 910 nm, concomitant with the disappearance of the CT band associated with **3** at 450 nm (Figure 7). Low-energy bands in this region have been observed in 4C planar Ni(III) complexes with N_2S_2 dicarboxamido-dithiolato coordination and were attributed to S-to-Ni(III) CT transitions,[44] a common spectroscopic feature for Ni(III)-N/S coordination complexes. Interestingly, Ni(II)-N_2S_2 complexes containing *o*-aminothiophenolate ligands with radical character also exhibit a low-energy band in a similar range in their UV-vis spectra. However, it must be noted that these bands are observed for the Ni-coordinated *o*-iminosemiquinonato form that would require the loss of two protons and one electron from the original *o*-aminothiophenol (see Chart S1 in the SI).[66] A close structural comparison of the C−C (avg: 1.397 ± 0.011 Å), C−S (1.773 Å), and C−N (1.392 Å) distances of S_{exo} in **2** and, by analogy, **3** did not reveal any contraction in the C−N (1.348 Å), C−S (1.724 Å) distances nor the quinoid structure (average = 1.405 ± 0.0226 Å) typical of a *o*-iminosemiquinonate and are more consistent with a coordinated thiophenolate anion[71] (see Chart S1 in the SI). It is thus unlikely that an N,S-coordinated *o*-iminosemiquinonate is present in $\mathbf{2}^{ox}$ or $\mathbf{3}^{ox}$. However, spectroscopically characterized metal-thiyl complexes with thiophenolate ligands of Ni(II) (λ = 670−800 nm in CH_2Cl_2),[72] Co(III) (λ = 780 nm in CH_2Cl_2),[73] Ru(III) (λ = 850 nm in acetone),[74] and V(IV) (λ = 910 nm in MeCN)[75] exhibit broad and distinct low-energy bands similar to $\mathbf{3}^{ox}$. These are significantly red-shifted from the broad transition observed for the free phenylthiyl radical (λ = 460−500 nm) generated by pulse radiolysis in pH 11 aqueous solution.[71] Most of these metal-thiyl complexes have been observed at low temperature, due to rapid formation of the disulfide, which is not surprising considering the second-order decay rate for disulfide formation from free $PhS^\bullet$ ($k = 9.6 \times 10^9$ M^{-1} s^{-1}).[71] These facts make the spectroscopic observation of $\mathbf{3}^{ox}$ even more noteworthy, in that this species is stable for hours at 298 K. After 24 h in DMF, the green color of $\mathbf{3}^{ox}$ faded and the red precipitate of **1** was isolated in ~70% yield.

An X-band EPR spectrum was collected for *in situ*-generated $\mathbf{3}^{ox}$ at 10 K in a DMF glass and is shown in Figure 7, along with a simulated fit. According to the simulation, the three *g*-values observed are g = 2.132 ($\sim g_\parallel$), 2.028, and 2.004 (g_{avg} = 2.055; $g_\perp \approx$ 2.016) with line widths of 35, 30, and 45 MHz, respectively. The typical EPR pattern for Ni(III), as seen in complexes that unambiguously contain Ni(III), such as Ni^{III}F430M,[76] the oxidized cofactor from methyl coenzyme M reductase (MCR), and a wide variety of Ni(III) tetraazamacrocyclic[77,78] and amino acid[79,80] complexes, can be described by $g_\perp \approx$ 2.2−2.3 and $g_\parallel$ = 2.00, which arise from a low-spin d^7 configuration with the single unpaired electron residing in the Ni d_{z^2} orbital.[80] EPR parameters for relevant, formally Ni(III) complexes are summarized in Table S2 in the SI. This classical Ni(III) EPR pattern is the reverse of that seen here for $\mathbf{3}^{ox}$, so the present complex cannot be an exclusive Ni(III) species with a $d_{z^2}^1$ ground state.

EPR spectra previously reported for Ni(III)−N_2S_2 complexes that more closely resemble **3** do not exhibit quite the classical pattern described above, as the symmetry of these complexes is often lower, leading to more rhombic EPR spectra, but most do have $g_\perp \approx$ 2.2−2.3 and $g_\parallel \approx$ 2.00.[10,36,43,44,81−83] Moreover, their spectra are more anisotropic with *g*-spreads, $g_{max} - g_{min} \approx 0.3$, as opposed to 0.128 for $\mathbf{3}^{ox}$, and with an overall greater deviation from the free electron (radical) *g* value (g_e = 2.00) than for $\mathbf{3}^{ox}$ (2.055), namely with $g_{avg} \approx$ 2.2.[10,36,44,81,83] The lower *g*-spread in $\mathbf{3}^{ox}$, smaller deviation from g_e, and ambiguous electronic ground state (see computational section below) would be more consistent with a coordinated S-radical with a smaller degree of electron delocalization onto the Ni *d*-orbitals, as observed in Ni-S_4 (bis-dithiolene) complexes,[84,85] than in classical Ni(III) complexes and even in other oxidized Ni(II) complexes with N_2S_2 donor sets. Thus, taken together, the UV-vis and EPR spectra support a Ni(III)-(SR) ↔ Ni(II)-($^\bullet$SR) description for $\mathbf{3}^{ox}$, rather than a genuine Ni(III)-SR species.

Low Temperature Absorption and MCD. The low temperature (4.5 K) absorption spectrum of $\mathbf{2}^{ox}$, generated by sparging **2** with $O_2(g)$ for 5 min, exhibited a broad band centered at ~22 000 cm^{-1} (455 nm) and a lower energy feature at ~10 000 cm^{-1} (1000 nm) (Figure 8, top). The MCD spectrum of this sample (Figure 8, bottom) exhibited negatively signed features corresponding to the bands observed in the low temperature absorption spectrum, as well as a prominent feature at ~16 000 cm^{-1} (625 nm). All MCD features increase in intensity with decreasing temperature, characteristic of *C*-

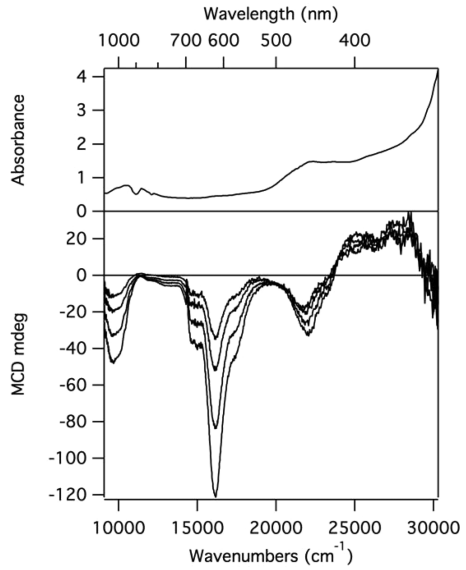

Figure 8. Low temperature absorption (4.5 K, top) and MCD (4.5, 8, 15, and 25 K, bottom) spectra of $\mathbf{2}^{ox}$ generated *in situ* by sparging **2** in a 1:4 (v/v) solvent mixture of MeCN and butyronitrile with $O_2(g)$ for 5 min.

DOI: 10.1021/ic503124f
Inorg. Chem. 2015, 54, 3815−3828

term behavior and indicative of a paramagnetic species. Note that the three features observed in the MCD spectrum of $\mathbf{2}^{ox}$ coincide with the three absorption bands observed at RT of *in situ*-generated $\mathbf{3}^{ox}$ (Figure 7), providing further evidence that $\mathbf{2}^{ox}$ and $\mathbf{3}^{ox}$ have nearly identical electronic structures. Given the relatively high intensities of the MCD features exhibited by $\mathbf{2}^{ox}$, it can be concluded that, in this species, and by analogy in $\mathbf{3}^{ox}$, significant unpaired spin density resides on the Ni atom. In support of this conclusion, the large ratio of MCD-to-absorption intensity of the feature at ~16 000 cm^{-1} (625 nm) indicates that the corresponding transition contains significant Ni $3d \rightarrow 3d$ character.

Computations. To obtain further insight into the geometric and electronic structures of $\mathbf{2}^{ox}$, DFT geometry optimization and property calculations were performed for a model of this species (termed $\mathbf{II}^{ox}$). An analogous geometry optimization for a model of the crystallographically characterized precursor **2** (model **II**) yielded Ni−ligand bond distances that agree reasonably well with the experimental values, thus validating our approach used to generate a model of the structurally ill-defined complex $\mathbf{2}^{ox}$ (Table 3). During the geometry optimization of $\mathbf{II}^{ox}$, the Ni atom retained a 4C planar geometry with Ni−ligand bond distances somewhat shorter than those in its one-electron reduced counterpart **II** (Table 3). A DFT calculation of the EPR parameters for $\mathbf{II}^{ox}$ yielded *g*-values of 2.16, 2.06, and 2.04, which agree well with the *g*-values determined experimentally for $\mathbf{3}^{ox}$ of 2.132, 2.028, 2.004 (Figure 7). Therefore, an analysis of the computed electronic structure description for $\mathbf{II}^{ox}$ is warranted.

Table 3. Ni−Ligand Bond Distances in DFT-Optimized Models of II and $\mathbf{II}^{ox}$, Compared with X-ray Crystallographically Determined Values for 2

	DFT		X-ray Structure of **2**
	II	$\mathbf{II}^{ox}$	$(Et_4N)[Ni(nmp)(SPh\text{-}o\text{-}NH_2)]$
$Ni-S_{exo}$	2.278	2.211	2.218
$Ni-S_{nmp}$	2.198	2.169	2.138
$Ni-N_{carboxamide}$	1.895	1.880	1.875
$Ni-N_{py}$	1.981	1.990	1.942

A comparison of the spin-up (α) and spin-down (β) manifolds of MOs obtained from a spin-unrestricted DFT calculation for $\mathbf{II}^{ox}$ (Figure 9) revealed that the βLUMO (βMO#93) corresponds to the formally singly occupied MO, as its α-counterpart (αMO#83, not shown) is occupied. To higher energy, the βLUMO+2 (βMO#95) can be identified as the Ni $3d_{x^2-y^2}$-based MO, while the βLUMO+1 (βMO#94) is mainly localized on the aryl-carboxamide moiety of the supporting nmp^{2-} ligand. As expected for a 4C planar complex, the occupied Ni $3d_{z^2}$-, $3d_{xy}$-, $3d_{xz}$-, and $3d_{yz}$-based orbitals (βMO#88, #87, #84, and #81, respectively) are significantly stabilized relative to the unoccupied Ni $3d_{x^2-y^2}$-based βMO#95.

The βLUMO has predominant S 3*p* (53% total: 26% from S_{exo} and 27% from S_{nmp}) and Ni 3*d* (21%; mainly $3d_{xz}$ and some $3d_{yz}$) orbital character, suggesting that the removal of an electron from **II** results in partial oxidation of both the thiolates and the Ni(II) ion. Consistent with this prediction, a plot of the spin density for $\mathbf{II}^{ox}$ shows that the unpaired electron is delocalized over the two S and the Ni atoms (Figure 9, inset). Consequently, our computational results obtained for $\mathbf{II}^{ox}$ indicate that $\mathbf{2}^{ox}$ is best described as a hybrid of [Ni(III)-($^-$SR)] ↔ [Ni(II)-(SR)] resonance structures. This description is in line with the intense MCD features and sizable *g*-spread displayed by $\mathbf{3}^{ox}$ relative to a free thiyl.

Reactivity of $\mathbf{3}^{ox}$ with Azide and Superoxide. The azide anion (N_3^-) is often employed as a redox-inert analogue of superoxide to obtain information on $M-O_2^{\bullet-}$ interactions. NiSOD shows no direct $Ni-N_3^-$ interaction based on EPR, UV-vis, and resonance Raman (rR) studies.[10,12] To evaluate the anion affinity of the Ni center in **3** and $\mathbf{3}^{ox}$, we added excess (10 equiv) NaN_3 to this NiSOD model and monitored its UV-vis spectrum. As observed for NiSOD, the UV-vis spectrum of **3** or $\mathbf{3}^{ox}$ did not change upon the addition of N_3^- (Figure 10), even after 1 h. Despite the presence of the potentially coordinating amine-N from S_{exo}, we tested whether the presence of 10 equiv of N-MeIm impacted any $Ni-N_3^-$ bonding. Indeed, the addition of N-MeIm resulted in a ~30 nm blue-shift in λ_{max} of **3** that may imply a Ni···N-MeIm interaction; however, no other direct evidence for a Ni-NMeIm bond was obtained. Analogous to the results in the absence of N-MeIm, no change was observed in the UV-vis spectrum when 10 equiv of N_3^- are added (Figure 10); thus, much like NiSOD, the Ni center in **3** and $\mathbf{3}^{ox}$ does not bind N_3^-.

To evaluate the potential of **3** and $\mathbf{3}^{ox}$ as SOD catalysts, experiments were performed with 18-crown-6 ether solubilized KO_2 in DMF at 298 K. Addition of a stoichiometric amount of KO_2 to a DMF solution of **3** resulted in no reaction, as monitored by UV-vis. However, the same reaction with *in situ* generated $\mathbf{3}^{ox}$ produced an immediate solution color change from green to red-brown. To obtain more information regarding the products formed in this reaction, fractional precipitation and isolation of the components present in the reaction mixture were performed (see Chart S2 in the SI). After vacuum distilling DMF from the reaction mixture, MeCN was added that afforded a red-orange precipitate and a brown MeCN-soluble portion. The MeCN-insoluble component was identified as the tetrameric species **1**, based on FTIR data. Two separate reactions of $\mathbf{3}^{ox}$ and $O_2^{\bullet-}$ revealed that the bulk of the Ni-nmp ends up as **1** (avg: 65% yield). Further attempts at separating components in the MeCN-soluble portion by selective precipitation with THF and Et_2O revealed the presence of **3** and the free unbound sulfinate (RSO_2^-) and sulfonate (RSO_3^-) of S_{exo} based on ESI-MS (see Figure S4 in the SI). Unfortunately, quantitative isolation of species other than **1** was not possible due to similar solubility profiles and the presence of CAN-related species. In addition, no $O_2(g)$ generation was observed utilizing electrochemical detection methods.[86] One can envision two primary reaction paths of $\mathbf{3}^{ox}$ with superoxide: (i) $O_2^{\bullet-}$ behaves as an outer-sphere reductant to furnish the corresponding Ni(II) complex **3** and O_2 (Scheme 3i), or (ii) $O_2^{\bullet-}$ oxygenates the S_{exo} atom of $\mathbf{3}^{ox}$ to generate the resulting sulfinate (RSO_2^-) and tetramer **1** (Scheme 3ii). Scheme 3i would be more in line with a Ni(III) assignment for $\mathbf{3}^{ox}$, whereas Scheme 3ii is more consistent with a Ni(II)-thiyl. However, one could envision the formation of similar products in both pathways if the product Ni(II) species **3** in Scheme 3i reacted with O_2 in a manner other than as an outer-sphere Ni(II) oxidant (i.e., "other products" in Scheme 3i). Either scenario explains the lack of any detectable $O_2(g)$ via electrochemistry, although the path in Scheme 3ii is more consistent with the significant amount of isolated **1** in the reaction mixture. Regardless of the path at work, these results advocate for a Ni(II)-thiyl assignment for $\mathbf{3}^{ox}$.

DOI: 10.1021/ic503124f
Inorg. Chem. 2015, 54, 3815−3828

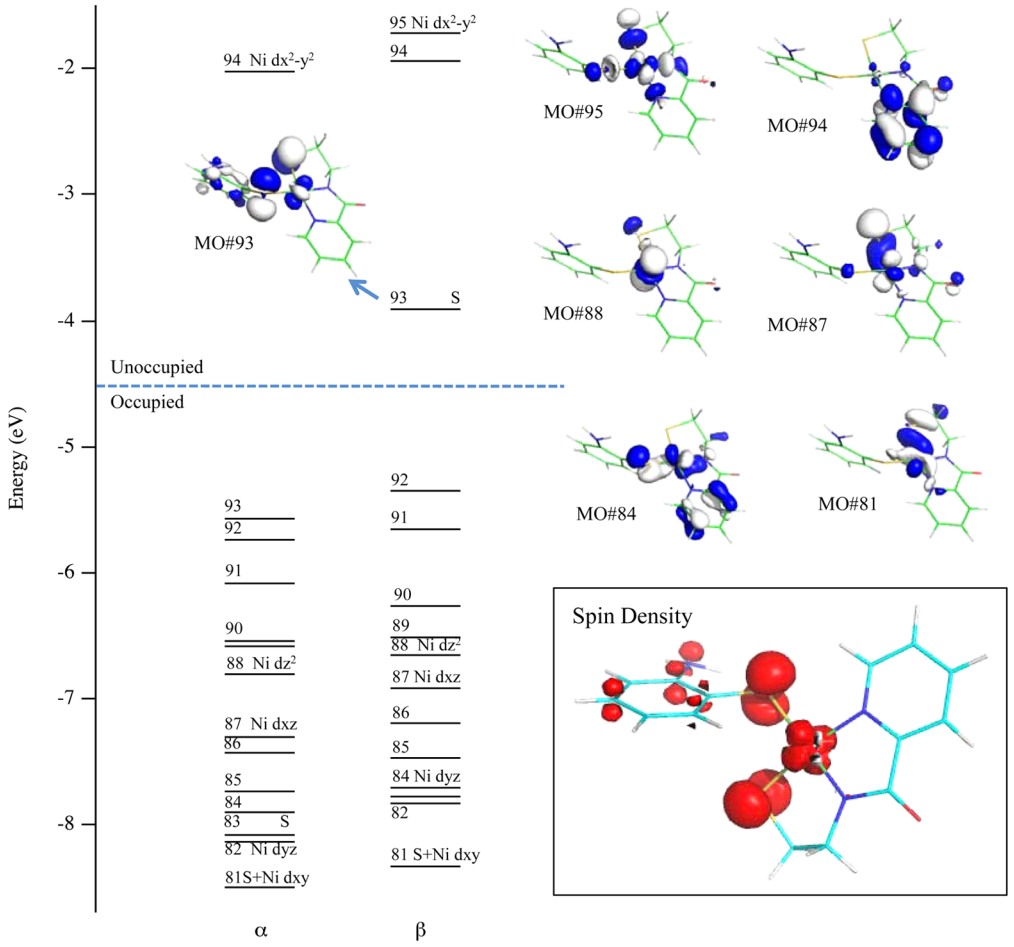

Figure 9. Relevant portion of the MO diagram and isosurface plots of select βMOs obtained from a spin-unrestricted DFT calculation for $\mathbf{II}^{ox}$. Inset: Spin density plot for $\mathbf{II}^{ox}$ (red = positive spin density; white = negative spin density).

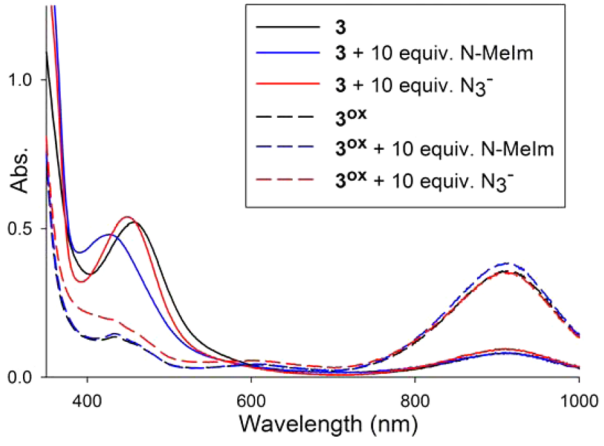

Figure 10. UV-vis spectra of **3** (black) and $\mathbf{3}^{ox}$ (black dash); **3** + 10 equiv N-MeIm (blue) and $\mathbf{3}^{ox}$ + 10 equiv N-MeIm (blue dash); **3** + 10 equiv N_3^- (red) and $\mathbf{3}^{ox}$ + 10 equiv N_3^- (red dash). All experiments were performed in DMF at 298 K.

CONCLUSIONS

In summary, we have prepared and characterized four Ni(II)-N/S complexes of the general formula $[Ni(N_2S)(SR')]^-$, where SR′ represents a site-differentiated location of the N_2S_2 coordination sphere as models of NiSOD. The SR′ ligand was functionalized with electron withdrawing substituents and/or a tethered N-donor in efforts to promote the formation of an oxidized Ni(III) complex that would be structurally and electronically analogous to the Ni–N_3S_2 coordination sphere of $NiSOD_{ox}$. We hypothesized that the incorporation of a weak N_{axial} ligand in SR′ from *o*-aminothiophenolate could mimic the long (2.3–2.6 Å) Ni-NHis bond in NiSOD and would be required to obtain such an oxidized species. Indeed, site-directed variants and DFT calculations revealed that the axial Ni-NHis bond in $NiSOD_{ox}$ is crucial for maintaining the rate ($k \approx 10^9$ M^{-1} s^{-1})[87,88] and appropriate electrochemical potential (0.090 V vs Ag/AgCl, pH 7.4, phosphate buffer) for turnover.[10,89] In addition, the few low molecular weight NiSOD models that access Ni(III) or that exhibit some SOD activity contain an N_{axial} ligand.[27,34,35] Chemical oxidation of NiSOD models **4** and **5** that lack this potential N-donor resulted in the quantitative formation of **1** and the disulfide (R′SSR′) of the monodentate thiolate. This result was not too surprising, given the expected high percentage of S-character in the HOMO of such Ni(II)-N_2S_2 complexes, although we had initially anticipated the electron-deficient thiolate in **5** would prevent such chemistry. Chemical oxidation of models **2** and **3** that contain a potential N-donor ligand resulted in the transient formation of an oxidized species ($\mathbf{2}^{ox}$ and $\mathbf{3}^{ox}$) that is best described as a resonance hybrid of a Ni(III)-thiolate and Ni(II)-thiyl species: [Ni(III)-(SR)] ↔ [Ni(II)-(•SR)]. This assignment was confirmed through a variety of experimental (X-ray, UV-vis, MCD, EPR, reactivity) and theoretical (DFT) techniques. These results may at first appear incongruent with

DOI: 10.1021/ic503124f
Inorg. Chem. 2015, 54, 3815–3828

Scheme 3. Possible Scenarios for the Reaction of 3^{ox} with Superoxide

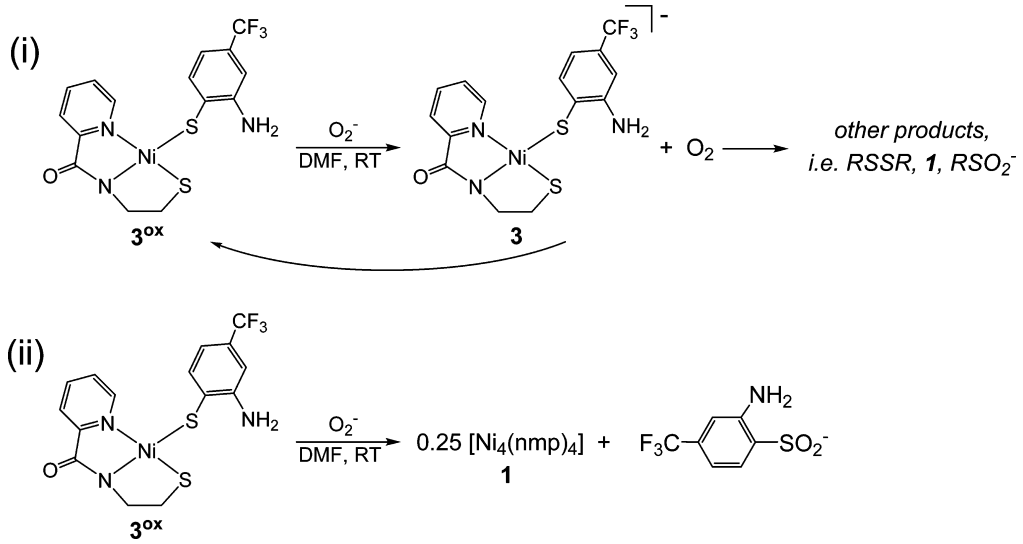

the actual mechanism of NiSOD. Most experimental work supports an outer-sphere electron transfer mechanism for $O_2^{\bullet-}$ disproportionation with the Ni(III/II) center possibly remaining 5C throughout catalysis.[8,39,40] In the first turnover, conversion of 4C $NiSOD_{red}$ to 5C $NiSOD_{ox}$ likely results in a 4C planar intermediate ($NiSOD_{ox}$-His_{off}) before formation of $NiSOD_{ox}$ due to the kinetics of electron transfer versus Ni–N(His) bond formation. Although this transient species has never been observed experimentally, DFT computations on $NiSOD_{ox}$-His_{off} indicate a predominant Ni-based HOMO and support a Ni(III) oxidation state (vide supra) even before axial His1 binding. This assignment is in contrast to the Ni(III)-thiolate ↔ Ni(II)-thiyl resonance description for the NiSOD models $\mathbf{2}^{ox}$ and $\mathbf{3}^{ox}$. However, $^{\bullet}$S(Cys) radicals have been observed in other enzymes,[90] some of which function through such a radical species.[91−97] Based on the EPR spectrum, Ni exists in the 3+ state in $NiSOD_{ox}$ with no indications of a coordinated $^{\bullet}$S(Cys), but the results presented here suggest that the transition from $NiSOD_{red}$ to $NiSOD_{ox}$-His_{off} may go through a Ni-stabilized/coordinated $^{\bullet}$S(Cys).

■ ASSOCIATED CONTENT

Supporting Information

Additional structural data for **1**, **2**, and **4** including CIF files, CVs of **2**, **3**, and **4**, a table of selected EPR-active Ni complexes, the flowchart and ESI-MS workup of the reaction of $\mathbf{3}^{ox}$ + KO_2, and the ^{1}H NMR and high-resolution ESI-MS of **2**–**5** are provided as Supporting Information. This material is available free of charge via the Internet at http://pubs.acs.org.

■ AUTHOR INFORMATION

Corresponding Author

*E-mail: tharrop@uga.edu.

Author Contributions

The manuscript was written through contributions of all authors. All authors have given approval to the final version of the manuscript.

Notes

The authors declare no competing financial interest.

■ ACKNOWLEDGMENTS

T.C.H. acknowledges financial support from a National Science Foundation CAREER Award (No. CHE-0953102) and the Office of the Vice President for Research (OVPR) and the Office of the Provost at the University of Georgia (UGA). T.C.B. acknowledges financial support by the National Institutes of Health (Grant No. GM 64631). S. D. acknowledges the NIH (Grant No. T32-GM008505) for support and the NSF (Grant No. CHE-0840494) for computational resources.

■ REFERENCES

(1) Valentine, J. S.; Wertz, D. L.; Lyons, T. J.; Liou, L.-L.; Goto, J. J.; Gralla, E. B. *Curr. Opin. Chem. Biol.* **1998**, *2*, 253–262.
(2) Miller, A.-F. *Curr. Opin. Chem. Biol.* **2004**, *8*, 162–168.
(3) McCord, J. M. In *Critical Reviews of Oxidative Stress and Aging: Advances in Basic Science, Diagnostics, and Intervention*; Rodriguez, H., Cutler, R., Eds.; World Scientific Publishing Co. Pte., Ltd.: Singapore, 2003; pp 883–895.
(4) De Leo, M. E.; Borrello, S.; Passantino, M.; Palazzotti, B.; Mordente, A.; Daniele, A.; Filippini, V.; Galeotti, T.; Masullo, C. *Neurosci. Lett.* **1998**, *250*, 173–176.
(5) Kocatürk, P. A.; Akbostanci, M. C.; Tan, F.; Kavas, G. Ö. *Pathophysiology* **2000**, *7*, 63–67.
(6) Maritim, A. C.; Sanders, R. A.; Watkins, J. B., III. *J. Biochem. Mol. Toxicol.* **2003**, *17*, 24–38.
(7) Fortunato, G.; Pastinese, A.; Intrieri, M.; Lofrano, M. M.; Gaeta, G.; Censi, M. B.; Boccalatte, A.; Salvatore, F.; Sacchetti, L. *Clin. Biochem.* **1997**, *30*, 569–571.
(8) Sheng, Y.; Abreu, I. A.; Cabelli, D. E.; Maroney, M. J.; Miller, A.-F.; Teixeira, M.; Valentine, J. S. *Chem. Rev.* **2014**, *114*, 3854–3918.
(9) Miller, A.-F. *FEBS Lett.* **2012**, *586*, 585–595.
(10) Fiedler, A. T.; Bryngelson, P. A.; Maroney, M. J.; Brunold, T. C. *J. Am. Chem. Soc.* **2005**, *127*, 5449–5462.
(11) Wuerges, J.; Lee, J.-W.; Yim, Y.-I.; Yim, H.-S.; Kang, S.-O.; Carugo, K. D. *Proc. Natl. Acad. Sci. U.S.A.* **2004**, *101*, 8569–8574.
(12) Barondeau, D. P.; Kassmann, C. J.; Bruns, C. K.; Tainer, J. A.; Getzoff, E. D. *Biochemistry* **2004**, *43*, 8038–8047.
(13) Grapperhaus, C. A.; Darensbourg, M. Y. *Acc. Chem. Res.* **1998**, *31*, 451–459.
(14) Neupane, K. P.; Shearer, J. *Inorg. Chem.* **2006**, *45*, 10552–10566.
(15) Shearer, J.; Long, L. M. *Inorg. Chem.* **2006**, *45*, 2358–2360.

DOI: 10.1021/ic503124f
Inorg. Chem. 2015, 54, 3815–3828

(16) Tietze, D.; Breitzke, H.; Imhof, D.; Kothe, E.; Weston, J.; Buntkowsky, G. *Chem.—Eur. J.* **2009**, *15*, 517−523.
(17) Tietze, D.; Tischler, M.; Voigt, S.; Imhof, D.; Ohlenschläger, O.; Görlach, M.; Buntkowsky, G. *Chem.—Eur. J.* **2010**, *16*, 7572−7578.
(18) Tietze, D.; Voigt, S.; Mollenhauer, D.; Tischler, M.; Imhof, D.; Gutmann, T.; González, L.; Ohlenschläger, O.; Breitzke, H.; Görlach, M.; Buntkowsky, G. *Angew. Chem., Int. Ed.* **2011**, *50*, 2946−2950.
(19) Shearer, J. *Angew. Chem., Int. Ed.* **2013**, *52*, 2569−2572.
(20) Shearer, J.; Peck, K. L.; Schmitt, J. C.; Neupane, K. P. *J. Am. Chem. Soc.* **2014**, *136*, 16009−16022.
(21) Krause, M. E.; Glass, A. M.; Jackson, T. A.; Laurence, J. S. *Inorg. Chem.* **2010**, *49*, 362−364.
(22) Krause, M. E.; Glass, A. M.; Jackson, T. A.; Laurence, J. S. *Inorg. Chem.* **2011**, *50*, 2479−2487.
(23) Glass, A. M.; Krause, M. E.; Laurence, J. S.; Jackson, T. A. *Inorg. Chem.* **2012**, *51*, 10055−10063.
(24) Krause, M. E.; Glass, A. M.; Jackson, T. A.; Laurence, J. S. *Inorg. Chem.* **2013**, *52*, 77−83.
(25) Ma, H.; Chattopadhyay, S.; Petersen, J. L.; Jensen, M. P. *Inorg. Chem.* **2008**, *47*, 7966−7968.
(26) Ma, H.; Wang, G.; Yee, G. T.; Petersen, J. L.; Jensen, M. P. *Inorg. Chim. Acta* **2009**, *362*, 4563−4569.
(27) Lee, W.-Z.; Chiang, C.-W.; Lin, T.-H.; Kuo, T.-S. *Chem.—Eur. J.* **2012**, *18*, 50−53.
(28) Nakane, D.; Funahashi, Y.; Ozawa, T.; Masuda, H. *Chem. Lett.* **2010**, *39*, 344−346.
(29) Shearer, J.; Zhao, N. *Inorg. Chem.* **2006**, *45*, 9637−9639.
(30) Shearer, J.; Dehestani, A.; Abanda, F. *Inorg. Chem.* **2008**, *47*, 2649−2660.
(31) Mathrubootham, V.; Thomas, J.; Staples, R.; McCraken, J.; Shearer, J.; Hegg, E. L. *Inorg. Chem.* **2010**, *49*, 5393−5406.
(32) Gale, E. M.; Patra, A. K.; Harrop, T. C. *Inorg. Chem.* **2009**, *48*, 5620−5622.
(33) Gale, E. M.; Narendrapurapu, B. S.; Simmonett, A. C.; Schaefer, H. F., III; Harrop, T. C. *Inorg. Chem.* **2010**, *49*, 7080−7096.
(34) Gale, E. M.; Cowart, D. M.; Scott, R. A.; Harrop, T. C. *Inorg. Chem.* **2011**, *50*, 10460−10471.
(35) Gale, E. M.; Simmonett, A. C.; Telser, J.; Schaefer, H. F., III; Harrop, T. C. *Inorg. Chem.* **2011**, *50*, 9216−9218.
(36) Gennari, M.; Orio, M.; Pécaut, J.; Neese, F.; Collomb, M.-N.; Duboc, C. *Inorg. Chem.* **2010**, *49*, 6399−6401.
(37) Gennari, M.; Retegan, M.; DeBeer, S.; Pécaut, J.; Neese, F.; Collomb, M.-N.; Duboc, C. *Inorg. Chem.* **2011**, *50*, 10047−10055.
(38) Mullins, C. S.; Grapperhaus, C. A.; Frye, B. C.; Wood, L. H.; Hay, A. J.; Buchanan, R. M.; Mashuta, M. S. *Inorg. Chem.* **2009**, *48*, 9974−9976.
(39) Shearer, J. *Acc. Chem. Res.* **2014**, *47*, 2332−2341.
(40) Broering, E. P.; Truong, P. T.; Gale, E. M.; Harrop, T. C. *Biochemistry* **2013**, *52*, 4−18.
(41) Mullins, C. S.; Grapperhaus, C. A.; Kozlowski, P. M. *J. Biol. Inorg. Chem.* **2006**, *11*, 617−625.
(42) Neupane, K. P.; Gearty, K.; Francis, A.; Shearer, J. *J. Am. Chem. Soc.* **2007**, *129*, 14605−14618.
(43) Nakane, D.; Wasada-Tsutsui, Y.; Funahashi, Y.; Hatanaka, T.; Ozawa, T.; Masuda, H. *Inorg. Chem.* **2014**, *53*, 6512−6523.
(44) Fiedler, A. T.; Brunold, T. C. *Inorg. Chem.* **2007**, *46*, 8511−8523.
(45) Rosenfield, S. G.; Armstrong, W. H.; Mascharak, P. K. *Inorg. Chem.* **1986**, *25*, 3014−3018.
(46) Palermo, R. E.; Power, P. P.; Holm, R. H. *Inorg. Chem.* **1982**, *21*, 173−181.
(47) Belford, R. L.; Belford, G. G. *J. Chem. Phys.* **1973**, *59*, 853−854.
(48) Fulmer, G. R.; Miller, A. J. M.; Sherden, N. H.; Gottlieb, H. E.; Nudelman, A.; Stoltz, B. M.; Bercaw, J. E.; Goldberg, K. I. *Organometallics* **2010**, *29*, 2176−2179.
(49) *SMART v5.626: Software for the CCD Detector System*; Bruker AXS: Madison, WI, 2000.
(50) Walker, N.; Stuart, D. *Acta Crystallogr., Sect. A: Found. Crystallogr.* **1983**, *A39*, 158−166.
(51) Sheldrick, G. M. *SADABS, Area Detector Absorption Correction*; University of Göttingen: Göttingen, Germany, 2001.
(52) Sheldrick, G. M. *SHELX-97, Program for Refinement of Crystal Structures*; University of Göttingen: Göttingen, Germany, 1997.
(53) Sheldrick, G. M. *Acta Crystallogr., Sect. A: Found. Crystallogr.* **2008**, *A64*, 112−122.
(54) Sheldrick, G. M. *SHELXTL 6.1, Crystallographic Computing System*; Siemens Analytical X-Ray Instruments: Madison, WI, 2000.
(55) Burnett, M. N.; Johnson, C. K. *ORTEP-III*, Report No. ORNL-6895; Oak Ridge National Laboratory: Oak Ridge, TN, 1996.
(56) Neese, F. *Wiley Interdiscip. Rev. Comput. Mol. Sci.* **2012**, *2*, 73−78.
(57) Becke, A. D. *J. Chem. Phys.* **1993**, *98*, 5648−5652.
(58) Lee, C.; Yang, W.; Parr, R. G. *Phys. Rev. B: Condens. Matter Mater. Phys.* **1998**, *37*, 785−789.
(59) Schäfer, A.; Horn, H.; Ahlrichs, R. *J. Chem. Phys.* **1992**, *97*, 2571−2577.
(60) Neese, F. *Inorg. Chim. Acta* **2002**, *337*, 181−192.
(61) *The PyMOL Molecular Graphics System, Version 1.5.0.4*; Schrödinger, LLC: Cambridge, MA, 2002.
(62) Wachters, A. J. H. *J. Chem. Phys.* **1970**, *52*, 1033−1036.
(63) The Ahlrichs (*2d2fg*,*3p2df*) polarization functions were obtained from the TurboMole basis set library under ftp.chemie.unikarlsruhe.de/pub/basen Sc-Zn: 2*p* functions from ref 60, plus one *f*-function from the TurboMole library.
(64) Kutzelnigg, W.; Fleischer, U.; Schindler, M. *The IGLO Method: Ab Initio Calculation and Interpretation of NMR Chemical Shifts and Magnetic Susceptibilities*; Springer−Verlag: Berlin, Heidelberg, Germany, 1990; Vol. 23.
(65) Gampp, H.; Lippard, S. J. *J. Am. Chem. Soc.* **1983**, *22*, 357−358.
(66) Herebian, D.; Bothe, E.; Bill, E.; Weyhermüller, T.; Wieghardt, K. *J. Am. Chem. Soc.* **2001**, *123*, 10012−10023.
(67) Jeffrey, G. A. *An Introduction to Hydrogen Bonding*; 1st Edition; Oxford University Press, Inc.: New York, 1997.
(68) Antonello, S.; Daasbjerg, K.; Jensen, H.; Taddei, F.; Maran, F. *J. Am. Chem. Soc.* **2003**, *125*, 14905−14916.
(69) Chang, T. M.; Tomat, E. *Dalton Trans.* **2013**, *42*, 7846−7849.
(70) Krüger, H.-J.; Holm, R. H. *Inorg. Chem.* **1989**, *28*, 1148−1155.
(71) Tripathi, G. N. R.; Sun, Q.; Armstrong, D. A.; Chipman, D. M.; Schuler, R. H. *J. Phys. Chem.* **1992**, *96*, 5344−5350.
(72) Stenson, P. A.; Board, A.; Marin-Becerra, A.; Blake, A. J.; Davies, E. S.; Wilson, C.; McMaster, J.; Schröder, M. *Chem.—Eur. J.* **2008**, *14*, 2564−2576.
(73) Kimura, S.; Bill, E.; Bothe, E.; Weyhermüller, T.; Wieghardt, K. *J. Am. Chem. Soc.* **2001**, *123*, 6025−6039.
(74) Grapperhaus, C. A.; Poturovic, S. *Inorg. Chem.* **2004**, *43*, 3292−3298.
(75) Chang, Y.-H.; Su, C.-L.; Wu, R.-R.; Liao, J.-H.; Liu, Y.-H.; Hsu, H.-F. *J. Am. Chem. Soc.* **2011**, *133*, 5708−5711.
(76) Jaun, B. *Helv. Chim. Acta* **1990**, *73*, 2209−2217.
(77) Wieghardt, K.; Walz, W.; Nuber, B.; Weiss, J.; Ozarowski, A.; Stratemeier, H.; Reinen, D. *Inorg. Chem.* **1986**, *25*, 1650−1654.
(78) Gore, E. S.; Busch, D. H. *Inorg. Chem.* **1973**, *12*, 1−3.
(79) Wang, J.-F.; Kumar, K.; Margerum, D. W. *Inorg. Chem.* **1989**, *28*, 3481−3484.
(80) Lappin, A. G.; Murray, C. K.; Margerum, D. W. *Inorg. Chem.* **1978**, *17*, 1630−1634.
(81) Krüger, H.-J.; Peng, G.; Holm, R. H. *Inorg. Chem.* **1991**, *30*, 734−742.
(82) Green, K. N.; Brothers, S. M.; Jenkins, R. M.; Carson, C. E.; Grapperhaus, C. A.; Darensbourg, M. Y. *Inorg. Chem.* **2007**, *46*, 7536−7544.
(83) Hanss, J.; Krüger, H.-J. *Angew. Chem., Int. Ed.* **1998**, *37*, 360−363.
(84) Lim, B. S.; Fomitchev, D. V.; Holm, R. H. *Inorg. Chem.* **2001**, *40*, 4257−4262.
(85) Szilagyi, R. K.; Lim, B. S.; Glaser, T.; Holm, R. H.; Hedman, B.; Hodgson, K. O.; Solomon, E. I. *J. Am. Chem. Soc.* **2003**, *125*, 9158−9169.

DOI: 10.1021/ic503124f
Inorg. Chem. 2015, 54, 3815−3828

(86) Carvalho, N. M. F.; Antunes, O. A. C.; Horn, A., Jr. *Dalton Trans.* **2007**, *2007*, 1023−1027.
(87) Herbst, R. W.; Guce, A.; Bryngelson, P. A.; Higgins, K. A.; Ryan, K. C.; Cabelli, D. E.; Garman, S. C.; Maroney, M. J. *Biochemistry* **2009**, *48*, 3354−3369.
(88) Ryan, K. C.; Guce, A. I.; Johnson, O. E.; Brunold, T. C.; Cabelli, D. E.; Garman, S. C.; Maroney, M. J. *Biochemistry* **2015**, *54*, 1016−1027.
(89) Bryngelson, P. A.; Arobo, S. E.; Pinkham, J. L.; Cabelli, D. E.; Maroney, M. J. *J. Am. Chem. Soc.* **2004**, *126*, 460−461.
(90) Giles, N. M.; Giles, G. I.; Jacob, C. *Biochem. Biophys. Res. Commun.* **2003**, *300*, 1−4.
(91) Licht, S.; Gerfen, G. J.; Stubbe, J. *Science* **1996**, *271*, 477−481.
(92) Fontecave, M.; Ollagnier-de-Choudens, S.; Mulliez, E. *Chem. Rev.* **2003**, *103*, 2149−2166.
(93) Cutsail, G. E., III; Telser, J.; Hoffman, B. M. *Biochim. Biophys. Acta*, DOI:10.1016/j.bbamcr.2015.1001.1025 (published online: Feb. 14, 2015, accessed March 19, 2015).
(94) Grove, T. L.; Benner, J. S.; Radle, M. I.; Ahlum, J. H.; Landgraf, B. J.; Krebs, C.; Booker, S. J. *Science* **2011**, *332*, 604−607.
(95) Silakov, A.; Grove, T. L.; Radle, M. I.; Bauerle, M. R.; Green, M. T.; Rosenzweig, A. C.; Boal, A. K.; Booker, S. J. *J. Am. Chem. Soc.* **2014**, *136*, 8221−8228.
(96) Wang, J.; Woldring, R. P.; Román-Meléndez, G. D.; McClain, A. M.; Alzua, B. R.; Marsh, E. N. G. *ACS Chem. Biol.* **2014**, *9*, 1929−1938.
(97) Broderick, J. B.; Duffus, B. R.; Duschene, K. S.; Shepard, E. M. *Chem. Rev.* **2014**, *114*, 4229−4317.

DOI: 10.1021/ic503124f
Inorg. Chem. 2015, 54, 3815−3828